

SKBF
KBS

TEKNISK
RAPPORT

83-47

**Stress/strain/time properties of
highly compacted bentonite**

Roland Pusch

University of Luleå
Luleå May 1983

SVENSK KÄRNBRÄNSLEFÖRSÖRJNING AB / AVDELNING KBS

POSTADRESS: Box 5864, 102 48 Stockholm, Telefon 08-67 95 40

STRESS/STRAIN/TIME PROPERTIES OF
HIGHLY COMPACTED BENTONITE

Roland Pusch

Division of Soil Mechanics
University of Luleå
May 15, 1983

This report concerns a study which was conducted for SKBF/KBS. The conclusions and viewpoints presented in the report are those of the author(s) and do not necessarily coincide with those of the client.

A list of other reports published in this series during 1983 is attached at the end of this report. Information on KBS technical reports from 1977-1978 (TR 121), 1979 (TR 79-28), 1980 (TR 80-26), 1981 (TR 81-17) and 1982 (TR 82-28) is available through SKBF/KBS.

STRESS/STRAIN/TIME PROPERTIES
OF HIGHLY COMPACTED BENTONITE

LULEÅ MAY 15 1983

DIV. OF SOIL MECHANICS
UNIVERSITY OF LULEÅ

ROLAND PUSCH

CONTENTS

Page

SUMMARY

INTRODUCTION

1

1. CLAY MATERIAL

4

1.1 Microstructural properties

4

1.2 Structural water

6

2. STRESS/STRAIN/TIME BEHAVIOR OF CLAYEY SOILS

8

2.1 Shear strength

8

2.2 General soil creep theory

12

2.2.1 Mathematical model

12

2.3 Stress/strain behavior of dense bentonites

19

2.3.1 Scope of the study

19

2.3.2 Test equipment

19

2.3.3 The bentonite clay

21

2.3.4 Test program

21

2.3.5 Results

23

2.4 Further aspects of the creep equation

28

2.4.1 General

28

2.4.2 Evaluation of the major type of inter- particle bonds from creep tests

28

2.4.3 Evaluation of the physical state of interlayer water

30

2.5 Constitutive relationships of highly compacted bentonite

32

2.5.1 Object

32

2.5.2 The complete creep equation

32

2.5.3 Stress/strain relationships for the rock shear case

35

3.	SETTLEMENT OF CANISTER - 1:st APPLICATION	37
3.1	Definition	37
3.2	Calculation	37
4.	ROCK SHEAR DISPLACEMENT - 2:nd APPLICATION	41
4.1	Definition	41
5.	CONCLUSIONS	43
6.	ACKNOWLEDGEMENTS	44
7.	REFERENCES	45

APPENDIX - Computational Mechanics Centre "Cylinder
in Clay"; BEM calculation

SUMMARY

The rheological properties of highly compacted bentonite are of practical importance in two respects as concerns the KBS concepts. Thus, they are determinants of the settlement rate of the metal canisters in their deposition holes, and they govern the stress state of the canisters in the event of rock displacements.

The rather comprehensive research work in recent years on the physico-chemical nature of smectite-rich clays, points to the importance of the strongly mineral-adsorbed water for their bulk behavior. The impact of shear stresses on the microstructure is the key problem, which requires the formulation of a reasonable physical model as a basis of the derivation of mathematical analogies for time-dependent stress/strain relationships. In this paper, a recently developed creep theory based on statistical mechanics has been used to analyze a number of experimental creep curves, the conclusion being that the creep behavior of dense MX-80 bentonite is in agreement with the physical model, and that the average bond strength is within the hydrogen bond region. The latter conclusion thus indicates that interparticle displacements leading to macroscopic creep takes place in interparticle and intraparticle water lattices. These findings were taken as a justification to apply the creep theory to a prediction of the settlement over a one million year period. It gave an estimated settlement of 1 cm at maximum, which is of no practical significance.

The thixotropic and viscous properties of highly compacted bentonite present certain difficulties in the determination and evaluation of the stress/strain/time parameters that are required for ordinary elastic and elasto-plastic analyses. Still, these parameters could be sufficiently well identified to allow for a preliminary estimation of the stresses induced in the metal canisters by slight rock displacements. The analysis, which needs to be deepened in order to get a more realistic picture of the impact of

such displacements on the physical state of the canisters, suggests that a 1 cm rapid shear perpendicular to the axes of the canisters can take place without harming them.

INTRODUCTION

The Swedish KBS multibarrier concept for the disposition of highly radioactive, unreprocessed reactor waste products implies that copper canisters containing radioactive material be surrounded by dense Na bentonite clay (Fig.1). Repositories consisting of tunnel systems with drilled deposition holes for the canisters will be located at a minimum depth of 500 m in crystalline rock. The tunnels are going to be backfilled with sand/bentonite mixtures, applied and compacted by applying ordinary contractors' technique.

The highly compacted bentonite, which separates the canisters from the rock, serves several purposes:

- It exerts a stabilizing pressure on the confining rock so that rock fragments will not fall down and damage the canisters
- It slows down the rate of water flow around the canisters to practically standstill, whereby the corrosion and the ultimate migration of escaped radionuclides are minimized
- It penetrates and seals rock fractures which traverse the holes
- It offers a highly viscous, self-sealing envelope, which is expected to moderate canister stresses that may appear as a consequence of slight rock displacements.

The latter effect is indispensable for maximum reduction of stress effects. It is largely dependent on the deformation properties of the bentonite, particularly with respect to the influence of time. Also, the stress relaxation behavior of the bentonite is important in this respect.

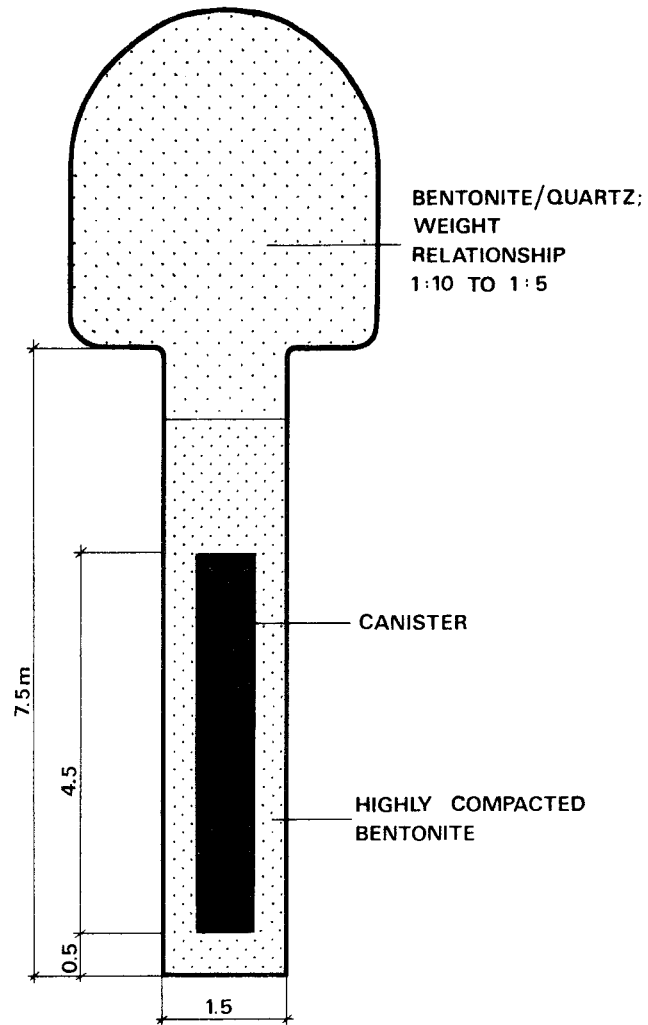


Fig.1. Cross section of tunnel with canister in drilled deposition hole.

Shear displacements in the rock, as illustrated by the schematic scenario in Fig.2, may result from tectonics or from stress alterations generated and triggered by excavation activities or thermal processes. Naturally, a stiff and brittle clay envelope would not yield much stress distribution in the metal canister, which instead calls for a rather soft clay consistency. If the clay is too soft, on the other hand, the heavy canister would displace it and ultimately come to rest directly on the rock, by which the isolating effect of the clay envelope is lost. Its rheological properties therefore have to be within certain limits, but it is clear that a sufficient bearing capacity and heat conductivity call for a high bulk density.

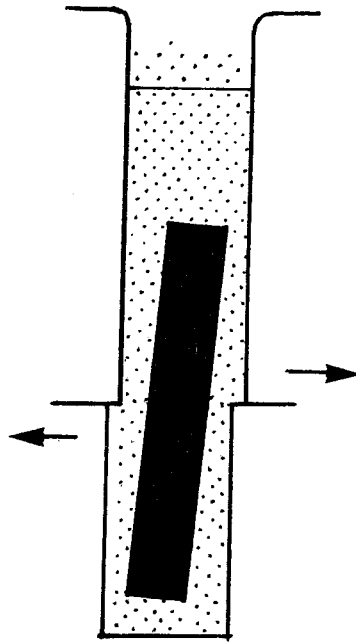


Fig.2. Rock shear displacement generating stresses in the canister.

1. CLAY MATERIAL

1.1 Microstructural properties

The required high density of the clay is achieved by compressing air-dry clay powder under high pressure. The clay material, which is preferably a Na smectite-rich bentonite, is applied in the form of well fitting blocks. The water content of such blocks is of the order of 10 %, the majority of the smectite flakes being collected in dense, silt-sized aggregates. Part of the voids contain air so that the degree of water saturation is approximately 50 - 60 %. After insertion in the deposition holes, the clay absorbs water from the rock, swells and fills the space between the canisters and the confining rock.

The swelling is associated with a successively improved degree of homogeneity which ultimately yields the microstructural state shown in Fig.3, at least in micro-elements. It illustrates a fairly isotropic system of smectite flakes, most of which are face-to-face oriented in stacks (domains) with a rather uniform interlayer distance. At a bulk density of water saturated MX-80 Na bentonite of 2.0 - 2.1 t/m³, which is representative of the KBS concepts, this distance is 5 - 7 Å theoretically, while in practice there may be a larger span. As an average, 2 to 3 water molecule layers will be hosted in the interlayer space, the large majority of the mineral contacts actually being established through such thin water films. Their properties will therefore become determinants of the physical behavior of the clay in bulk. Fig.4 shows a representative electron micrograph of "matured" MX-80 bentonite.

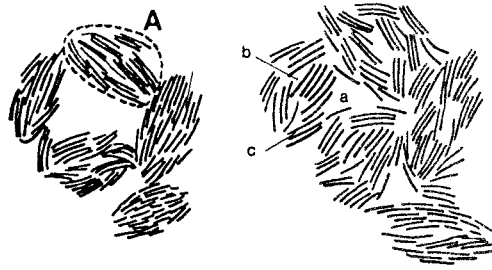


Fig.3. Schematic particle arrangement in dense bentonites. Left picture: powder grains in air-dry state. Right picture: "homogeneous" state after saturation and particle redistribution. A=particle aggregate, a=large interparticle void, b=small interparticle void, c=inter-lamellar space.

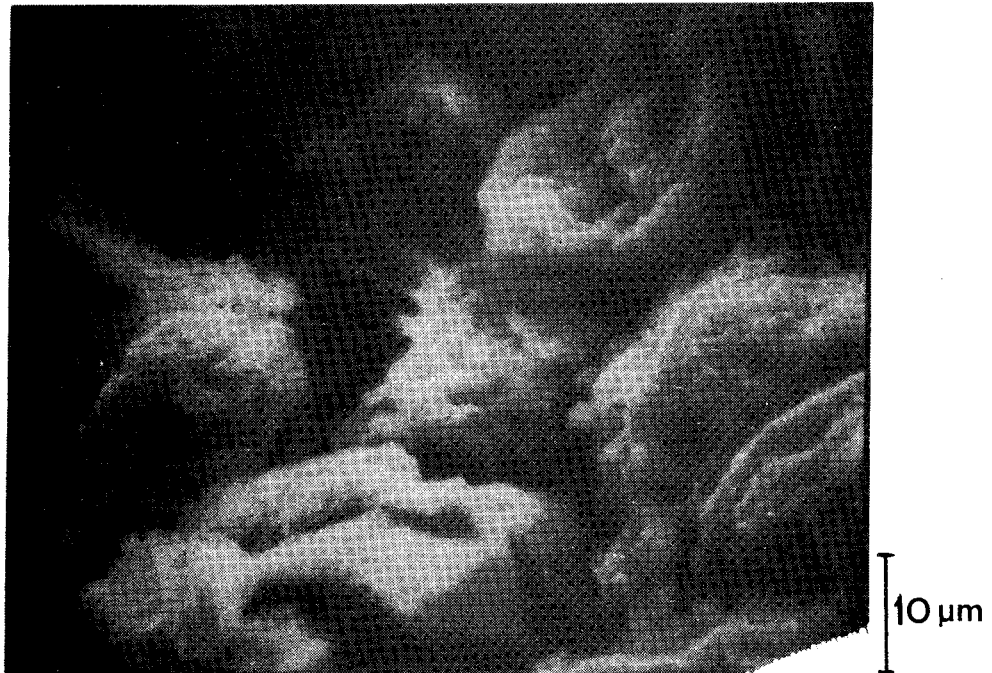


Fig.4. Scanning electron micrograph of dense MX-80 clay "matured" for 1 year. Bulk density 2.0 t/m^3 .

1.2 Structural water

The coupling of water molecules, mutually as well as to inter-crystalline smectite lattices, leads to a structural organization of adsorbed water which does not primarily depend on the presence of exchangeable cations. Such ions merely seem to give rise to well-defined structural modifications of the adsorbed water lattice (1). One possible structural model for montmorillonite, being the most common smectite group member, which allows for such lattice-associated water, is the EDELMAN & FAVEJEE concept shown in Fig.5. It differs from the traditional, earlier HOFMANN, ENDELL & WILM model, which does not readily account for such water adsorption, and which lacks some of the physico-chemical merits offered by the first-mentioned model. Applying the EDELMAN & FAVEJEE version, the organized water lattice can be visualized as in Fig.6, in which no. 3-6 are representative of most mineral "contacts" in dense bentonites.

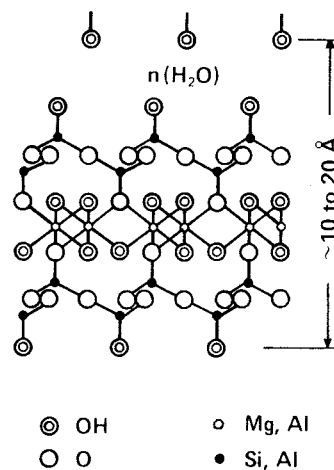
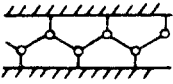
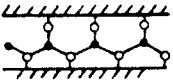
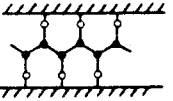
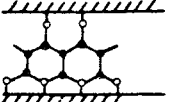
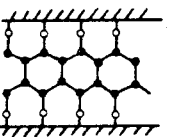
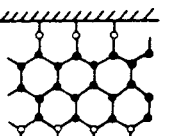
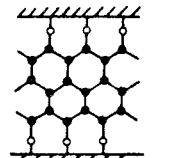


Fig.5. The EDELMAN & FAVEJEE montmorillonite crystal structure. $n(\text{H}_2\text{O})$ represents intercrystalline water and cations (1,2).

	Schematic interlayer structure	H ₂ O molecules per unit cell	Basal spacing, Å	g H ₂ O/g clay	mM H ₂ O/g clay	Remarks
0		0	12.30	0; 0,084 ^a	0; 4.667 ^a	Unstable; no hydration; four OH groups per unit cell
1		2.66	15.05	0.059	3.278	Unstable
2		5.33	17.81	0.119	6.661	Stable monolayer
3		8.0	18.73	0.179	9.944	Unstable
4		10.67	21.49	0.238	13.222	Stable; two layers
5		13.32	22.41	0.297	16.5	Unstable
6		16.0	25.17	0.357	19.833	Stable; three layers

^a At complete dehydroxylation.

Fig.6. Montmorillonite/water association (1).

The physical state of the adsorbed water is a determinant of its mechanical properties and therefore of the rheological behavior of the integrated mineral/water system. The matter is discussed later in this report.

2. STRESS/STRAIN/TIME BEHAVIOR OF CLAYEY SOILS

2.1 Shear strength

It is essential for the understanding of the stress/strain characteristics of "artificially" consolidated smectitic clays that their microstructure, including the distribution and arrangement of the crystallites as well as the continuity of organized water, is much more homogeneous than that of sedimented soft illitic clays. The latter are characterized by an obvious peak shear strength, except for shearing at very low strain rates, and this is caused by their collapsible microstructure which offers little resistance to shear once the peak value has been reached (Fig.7).

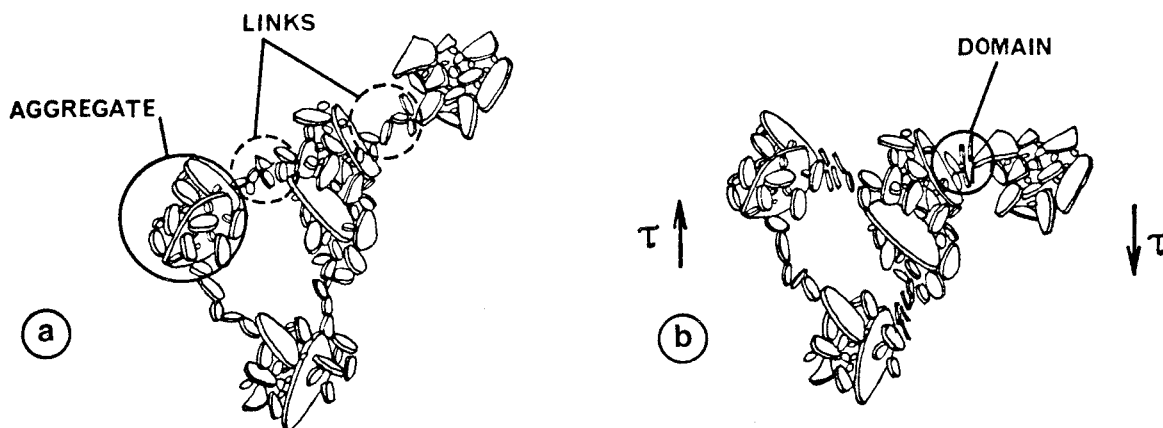


Fig.7. Structural distortion in sheared, aggregated clay. Domains are formed by local overstressing.

The difference in structural homogeneity is suitably expressed in terms of the shape of the activation energy spectrum for energy barrier transitions (cf. Fig.8). As will be shown later, the spectrum is a valuable tool in the analysis of the creep behavior of clays.

When local overstressing occurs in aggregated clay, a fraction of the atomic bonds are broken and a number of contacts are interrupted. This yields particle displacements leading to the formation of face-to-face-grouped particles, i.e. to domains (Fig.7). Their interparticle distances are adjusted to reach force equilibrium which involves expansion and separation of the flaky minerals. A certain strength gain may arise from successively formed interconnecting layers of adsorbed water, which actually produce the separation, but the expansion may be substantial in soft clays with much internal pore space, and the domains therefore remain to be the weakest structural members of aggregated clays.

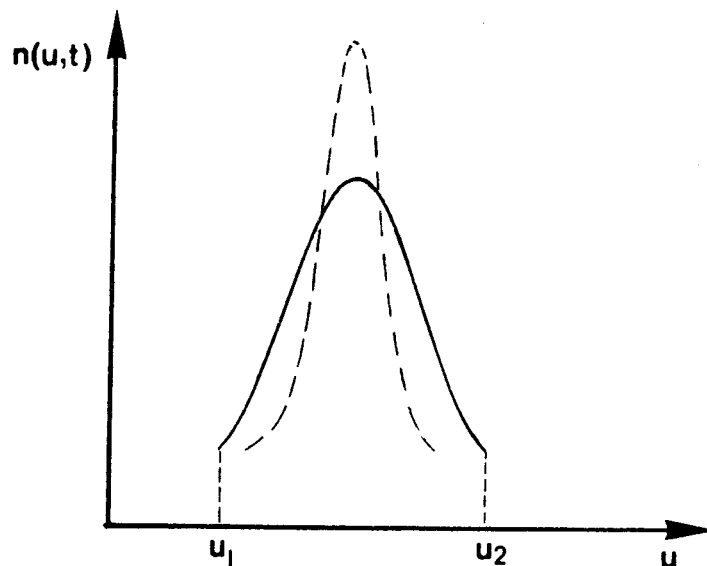


Fig.8. Activation energy spectrum at a given time t after the onset of creep. Full line represents aggregated clay with largely varying barrier heights u due to many kinds of particle bonds. Broken curve is typical of a more homogeneous clay with one dominant type of bonds (3).

It is logical to believe that further displacements in the clay network due to deviatoric stresses are mainly contributed by the domains and by the formation of additional weak components of the same kind. They are therefore considered as major slip units in the evolution of creep.

The weakness of the domains facilitates a relatively large initial deformation at the onset of creep, but several mechanisms combine to reduce this high rate, the main one being that initial slip induces displacements such that more bonds are activated and that stronger units make contact and help to strengthen the system. The displacements may generate additional domains from previous bridging links that are overstressed. If the stress level is sufficiently high, such structural damage will accumulate and bulk failure occurs soon after the load application or much later, in the form of creep failure. Shear failure is manifested by an accelerating strain rate followed by uncontrolled rapid mass flow and complete structural disorder if the sliding mass is free to move. This is a familiar situation in the case of unstable slopes and when shallow foundations are overstressed.

Considering the present case of a borehole with a canister embedded in clay, it is clear that only internal displacements can occur in the confined clay body. If the clay is sufficiently dense to dilate or to maintain a constant volume when affected by shear stresses, creep will be the only deformation mechanism. At high shear stresses the creep rate may be only slightly retarded, while at low and moderate stresses two healing processes oppose the weakening and retard the strain rate. They are due to the strain-induced interaction of adjacent aggregates and involve micro-dilatancy and mechanical interlocking, as well as reformation of water lattices and new interlinking particle groups. These processes take place when the mutual displacement of close aggregates has ceased, either because of interlocking or because they are temporarily not subjected to strain-inducing local stresses. The net effect of these "thixotropic" processes seem to depend somewhat on the strain rate. An indication of the correlated strengthening and weakening can be obtained from Fig.9.

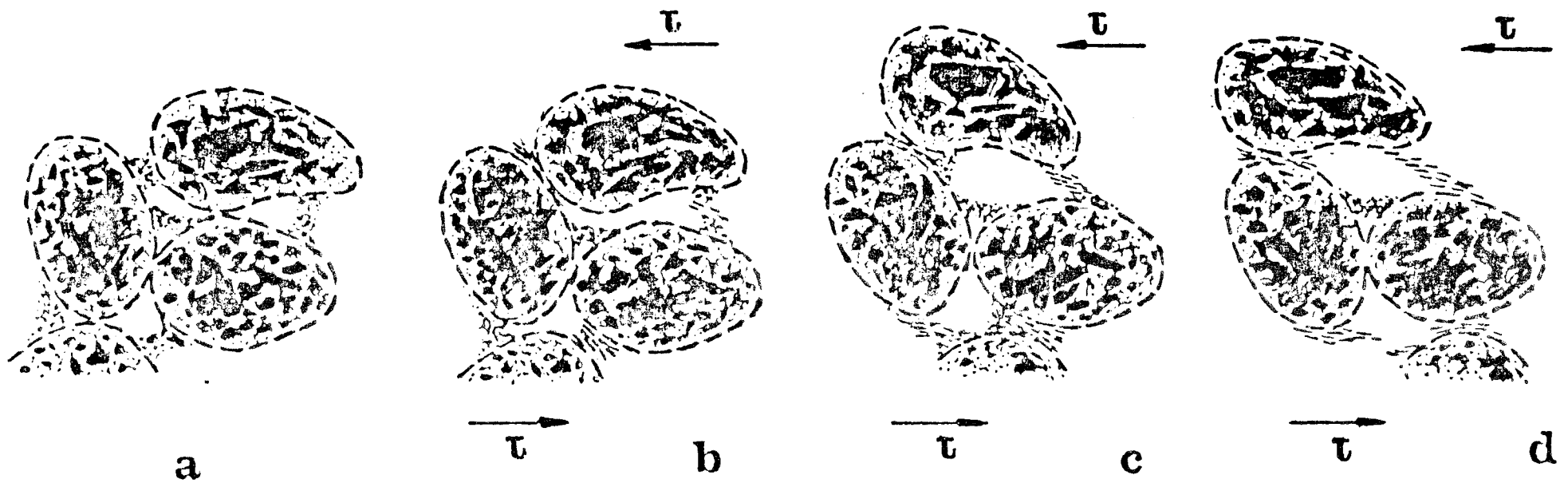


Fig.9. Schematic picture of consecutive stages in the evolution of the creep of aggregated clay. a) Before loading, (b) instantaneous shear and formation of domains, (c) additional domains are formed, accompanied by healing and breakdown, (d) creep failure.

As to the present case of a canister embedded in a very dense, structurally fairly homogeneous smectite, it is obvious that the virgin microstructure of this clay envelope is dominated by domains (cf. Fig.3). This means that healing due to interacting strong, structural units is less important than in aggregated clays but also that weakening through creep-induced domain formation is almost absent, which in turn would suggest a more Newtonian-like behavior. In practice, however, a matured bentonite of the MX-80-type will still be fairly aggregated and should therefore not behave very differently from illitic clays. A slightly more liquid-like appearance would still be expected, at least at low deviator stresses and this also turns out to be the case.

2.2 General soil creep theory

2.2.1 Mathematical model

The structural heterogeneity and bond strength variation as well as the use of the energy barrier concept suggest that a reasonable mathematical creep model should preferably be based on statistical mechanics. The general features of a relevant stochastic model which corresponds to our simplified physical model should then be:

1. There is a variation in activation energy for slip (Fig.8). The magnitude of the energy spectrum interval and the shape of the distribution curve reflect the microstructural density and heterogeneity and the type of bonds; hydrogen bonds, van der Waals bonds etc.
2. Each clay element contains a certain number of slip units in a given interval of the activation energy range.
3. In the course of the creep the low energy barriers are triggered early. New slip units come into action at the low activation energy end of the spectrum. This end represents a "generating barrier", while its upper end is an

"absorbing barrier".

4. The model must allow both for jumps which, when they take place, bring the given slip unit up against a barrier by an amount δu higher than the previous one, as well as for jumps which lead to reduced barrier heights.

The derivation of relevant mathematical expressions has been given previously by PUSCH & FELTHAM (4) to which the reader is referred. Only the basic steps of evolution will be given here.

At any given temperature only a limited energy spectrum $u_1 < u < u_2$ will be of significance in the determination of the creep rate. Concerning the form of the spectrum, which can be interpreted in terms of the number of potential slip units per unit volume held up by barriers of height u , this number is $n(u, t)\delta u$ where t is time after the onset of creep, and δu the energy interval into which we consider the spectrum to be divided.

A basic assumption is that the frequency of slips is given by the Arrhenius rate equation:

$$v(u) = v_D \exp(-u/kT) \quad (1)$$

where u is the barrier height and $v(u)$ the slip frequency, while v_D is an atomic vibrational frequency of the order of 10^{12} per second. k is Boltzmann's constant and T the absolute temperature.

If slip has been activated at a certain point, i.e. a barrier has been overcome, a contribution to the overall shear is made by the associated extension of the local slip-patch and the next barrier to be encountered by the same spreading slip-zone will be either higher or lower by an average amount δu . The magnitude of this unit is characteristic of the stress field and of the physical nature of the barriers.

It is reasonable to allow for an equal probability for slips to occur to the next higher or lower energy level, and considerations analogous to those familiar from the derivation of equations of diffusion (5) then yield, on writing n for $n(u,t)$:

$$\frac{\partial n}{\partial t} = D \left[\frac{\partial^2 [n \exp(-u/kT)]}{\partial u^2} \right] \quad (2)$$

$$D = 1/2 v_D (\delta u^2)$$

For low temperatures, i.e. less than about 100 degrees centigrade, the solution of Eq.2 yields:

$$n(u,t) \propto p \cdot \exp(-p) \quad (3)$$

with $p = \exp(u/kT)/v_D(t+t_0)$

$t_0 =$ constant of integration

The creep rate, in which we are interested, can be described and derived as follows.

If the passage of slip through the element of dimensions L (Fig.10) displaces the part above the slip plane by an amount b over the plane below the slip plane, then the resulting shear is b/L . If a slip unit does not traverse the whole element but a certain distance on making an activated slip under the influence of the local stress field, and thereby produces displacements over an area A^*/L^2 times smaller than b/L , we find:

$$\delta_\gamma = \left(\frac{b}{L} \right) \left(\frac{A^*}{L^2} \right) \quad (4)$$

Thus, δ_γ would be equal to b/L only if the area A^* extended over the entire cross section.

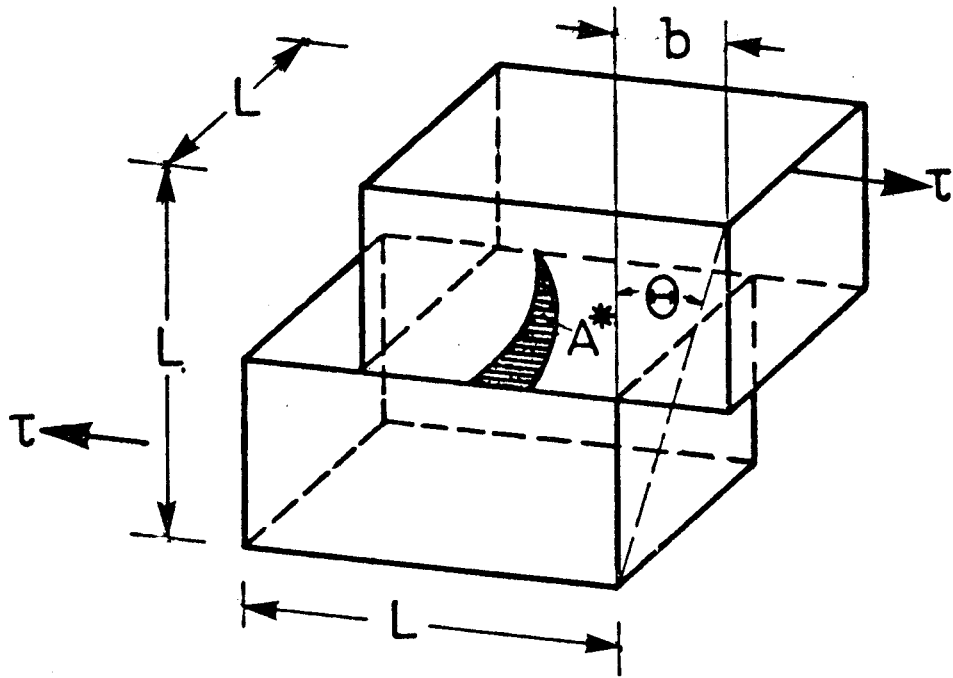


Fig.10. Clay element with internal displacement produced by a slip unit jump. τ is the shear stress.

If slip has been activated at a certain spot, the contribution to the overall shear strain is given by Eq.4. If there are $n\delta u$ points per unit volume and unit of energy where the barrier height is u , then in a cubical element with edge dimensions L , the contribution $\delta\gamma_u$ due to slip of all u -units is:

$$\delta\gamma_u = \left[n(u, t) L^3 \right] \left(\frac{b}{L} \right) \cdot \frac{A^*}{L} \delta u \quad (5)$$

If the number of slips at such points is $\nu e^{-u/kT}$ per second, where $\nu = \nu(u)$, then the contribution by the considered u -interval to the strain rate is:

$$\delta\dot{\gamma} = \nu b A^* n(u, t) \exp(-u/kT) \delta u \quad (6)$$

If each activated slip gives the same, average contribution A^* to the bulk shear strain of the specimen, then the creep rate, expressed here as the axial strain rate of a triaxially loaded cylindrical specimen, will be:

$$\begin{aligned} \dot{\epsilon} &= b \cdot A^* \int_{u_1}^{u_2} v(u) \cdot n(u, t) du = \\ &= b \cdot A^* v_D \int_{u_1}^{u_2} n(u, t) \cdot \exp(-u/kT) du \end{aligned} \quad (7)$$

The model is thus seen to be compatible with the processes illustrated in Fig.9, i.e. the lower end of the energy spectrum may relate mainly to the deformation of the domains, while higher barriers will be associated with more rigid components of the system.

The range of u -values terminates at u_1 at the low u -end, while u_2 represents the upper limit of the operative spectrum. Slip with the associated change in energy barrier height takes place over the entire spectrum except that no outflow to lower levels than u_1 or higher than u_2 take place. u_1 is a "generating barrier" so that new units provide a net inflow from outside the spectrum into its lower end, which is required by our third criterion and which is an essential property of the physical model. It simply means that new domains, formed favorably in regions where the activation energy for slip is low, come into action. u_2 represents strong bonds, and slips which bring the slip unit up against barriers higher than u_2 will occur with such a low frequency that their contribution to the creep over the considered period of time may be neglected. u_2 may therefore be regarded as an "absorbing barrier".

Combination of Eqs.3 and 7 yields - neglecting higher order terms (5) - the general creep equation:

$$\dot{\epsilon} \propto (t+t_0)^{-1} \quad (8)$$

which is the creep equation we will consider.

The significance of t_0 may be understood by considering that in the course of applying the deviatoric stress, at the onset of creep, the stress rises from zero to its nominal, final value. A u -distribution will therefore exist at $t = 0$, i.e. immediately after the full load is reached. t_0 is thus characteristic of the structure of the "pre-strained" material, high t_0 's indicating much structural damage in aggregated clays or large initial strain in "viscous"-type soils such as mud and relatively soft smectitic clay.

Fig.11 is a graphical representation of Eq.8. With the applied log divisions, the straight line represents creep with $t_0 = 0$, while the broken curve implies $t_0 > 0$.

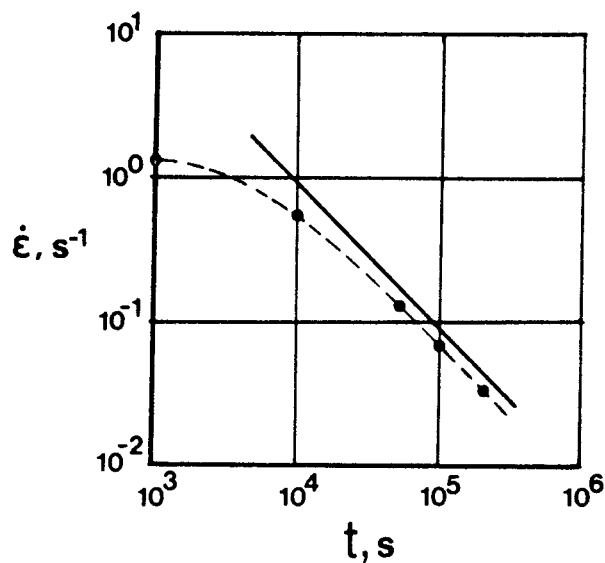
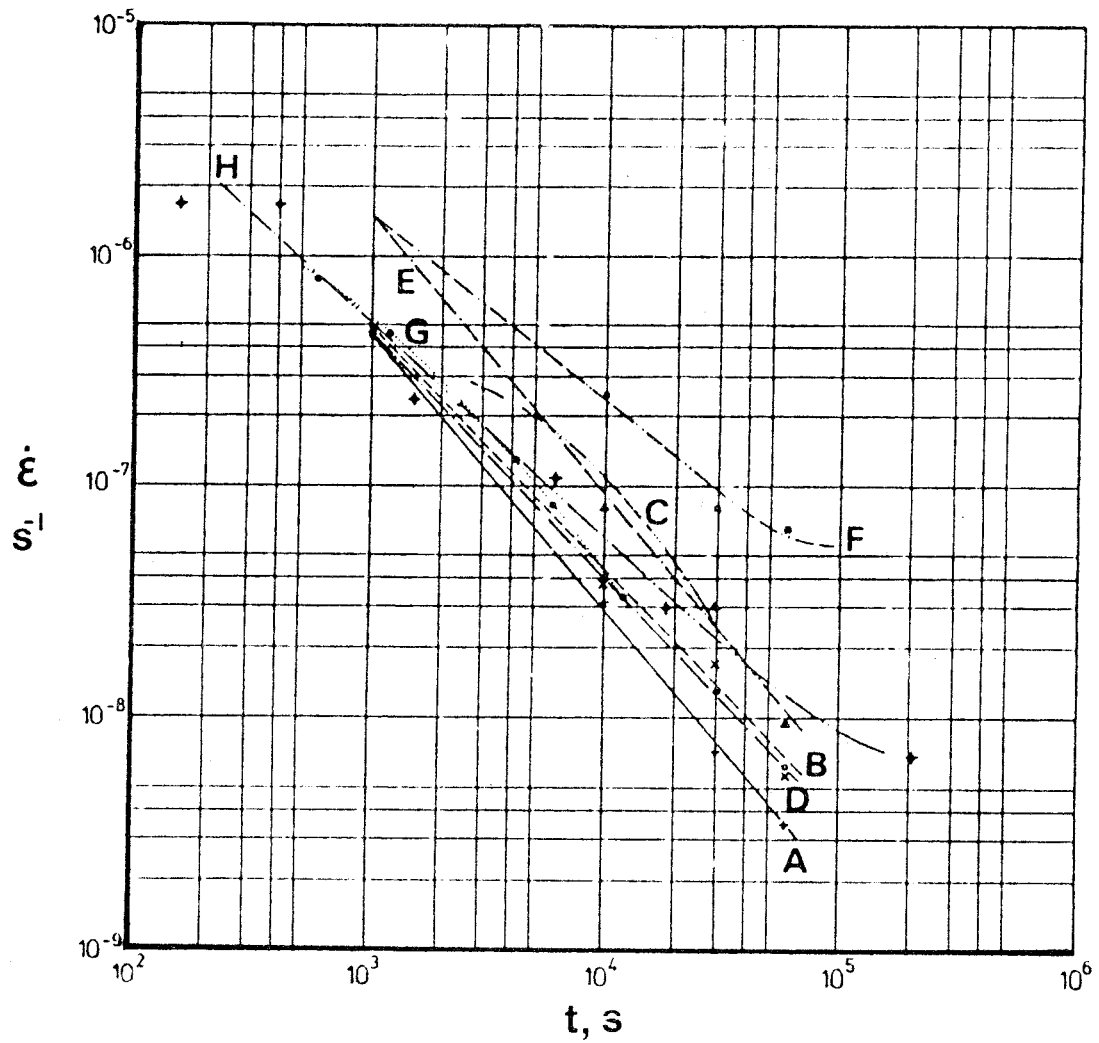


Fig.11. Creep curves according to Eq.8. Straight line for $t_0=0$, broken curve $t_0>0$.



LEGEND

	CLAY	TYPE	w%	g _o %	STRESS LEVEL	TEST	
—	+	A	MARINE	81	0.5	D _f /3	UNCONF., DRAINED
- - -	o	B	BRACKISH	92	1.5	D _f /3	" "
- · - · -		C	FRESH W.	70	1.0	D _f /3	" "
- · - · -	x	D	MARINE	86	1.0	D _f /3	" "
- · - · -	△	E	FRESH W.	72	2.0	D _f /3	" "
- · - · -	•	F	FRESH W.	114	4.0	D _f /3	" "
·····	•	G	FRESH W.	100	1.0	3/4D _f	TRIAX., UNDRAINED
- · - · -	♦	H	MARINE	93	1.0	3/4D _f	" "

1) D_f = Deviator stress at failure g_o = Organic content

Fig.12. Creep curves of Quaternary, soft, illitic clays (Author's compilation).

The logarithmic type of soil creep is typical and the applicability of Eq.8 appears to be of wide scope, which is probably a consequence of its stochastic and thermodynamic implications (6). Thus, at low and moderate stress levels, soft as well as stiff clays of various origin exhibit an amazingly close grouping of the creep curves with the strain rate being inversely proportional to the time after the onset of creep (Fig.12).

2.3 Stress/strain behavior of dense bentonite

2.3.1 Scope of the study

It appears from the preceding text that shear strain of the completely confined clay bodies in their deposition holes with the canisters, will be the main deformation mechanism. Relevant parameters would be the maximum shear stress that the clay can take, i.e. the shear strength, and the creep properties.

The main object of this study was to identify the creep characteristics of dense bentonite and to determine relevant creep parameter values in order to predict the rate of canister settlement as well as to make a general estimate of the stress-distributing power of the clay in the case of rock displacements according to Fig.2. Laboratory experiments, forming the basis of computer calculation of the settlement and of the stresses induced by the rock shear, were run for this purpose; they are reported in some detail in the subsequent text.

2.3.2 Test equipment

Triaxial testing is the most suitable technique for creep studies since the stress conditions are reasonably well known. However, dense, expansive clays present considerable difficulties because of the high cell pressures that have to be applied. Thus, taking the effective pressure to be equivalent to the swelling pressure (7), the cell pressure has to be in the interval of 3 to 30 MPa for bulk densities ranging between 1.9 and 2.1 t/m³.

The triaxial test equipment used in the present study could not be safely operated at higher cell pressures than about 10 MPa, which corresponds to a bulk density of slightly more than 2 t/m^3 . This value was therefore set as the upper limit of the presently investigated density range.

Pilot tests showed that undrained conditions gave almost the same creep data as drained, which is explained by the very low permeability ($k < 5 \cdot 10^{-13} \text{ m/s}$), and some of the tests were therefore run as undrained, constant shear stress tests with pore pressure readings. Since no consolidation of the clay is expected under real conditions, such tests as well as drained ones are relevant.

The \varnothing 50 mm, 100 mm long samples were prepared in swelling pressure oedometers by the standard procedure (8), i.e. by compacting air-dry bentonite powder to a pre-set density followed by water uptake under constant volume conditions. They were then transferred to the triaxial cell and sealed from the pressure fluid by rubber membranes. The cell pressure was successively adjusted, keeping the sample drainage open, until the samples reached equilibrium manifested by a constant volume. In this state, which was usually reached after one or two weeks, the swelling pressure was exactly balanced by the cell pressure. Thus, the procedure offered a nice way of checking the swelling pressures obtained from large test series using oedometers, the agreement between the two sets of results being fairly good.

In the undrained tests, the drainage was then closed and a constant stress applied through a lever arrangement (Fig.13). The shortening of the sample, i.e. the deformation in the direction of the major principal stress, was recorded by use of a transducer.

Tests were run at room temperature as well as at elevated temperatures (50 and 90 degrees centigrade), the heating being arranged by submerging the entire cell in a uniformly heated bath. The influence of heat on the various measuring and loading devices was checked and properly accounted for in the evaluation of the tests.

2.3.3 The bentonite clay

The KBS reference bentonite material MX-80 was used in the present study and it was saturated with synthetic "Allard" groundwater. The mineral composition, granulometric characteristics etc. of this clay material have been reported previously (9). In short, the clay content (minus 2 micrometers) ranges between 80 and 90 %, and 80 to 90 % of this fraction is montmorillonite. The composition of the very slightly brackish Allard water (91 mg of cations and 215 mg of anions per liter) is also fully described in earlier reports (10).

2.3.4 Test program

The tedious preparation of samples and required long testing period for certain representative sets, limited the extension of the study and so far only 8 tests have been completed. The main data are given in Table 1.

Table 1. Test data

Test no.	Bulk density t/m ³	Deviator stress kPa	Temperature C°
1 UD	2.0	2500	22
2 UP	2.0	400	22
3 UD	2.0	800	22
4 UD	1.9	400	22
5 UD	1.9	800	22
6 D	1.9	400	22
7 D	1.9	800	22
8 D	1.9	400	93

UD stands for undrained, D for drained

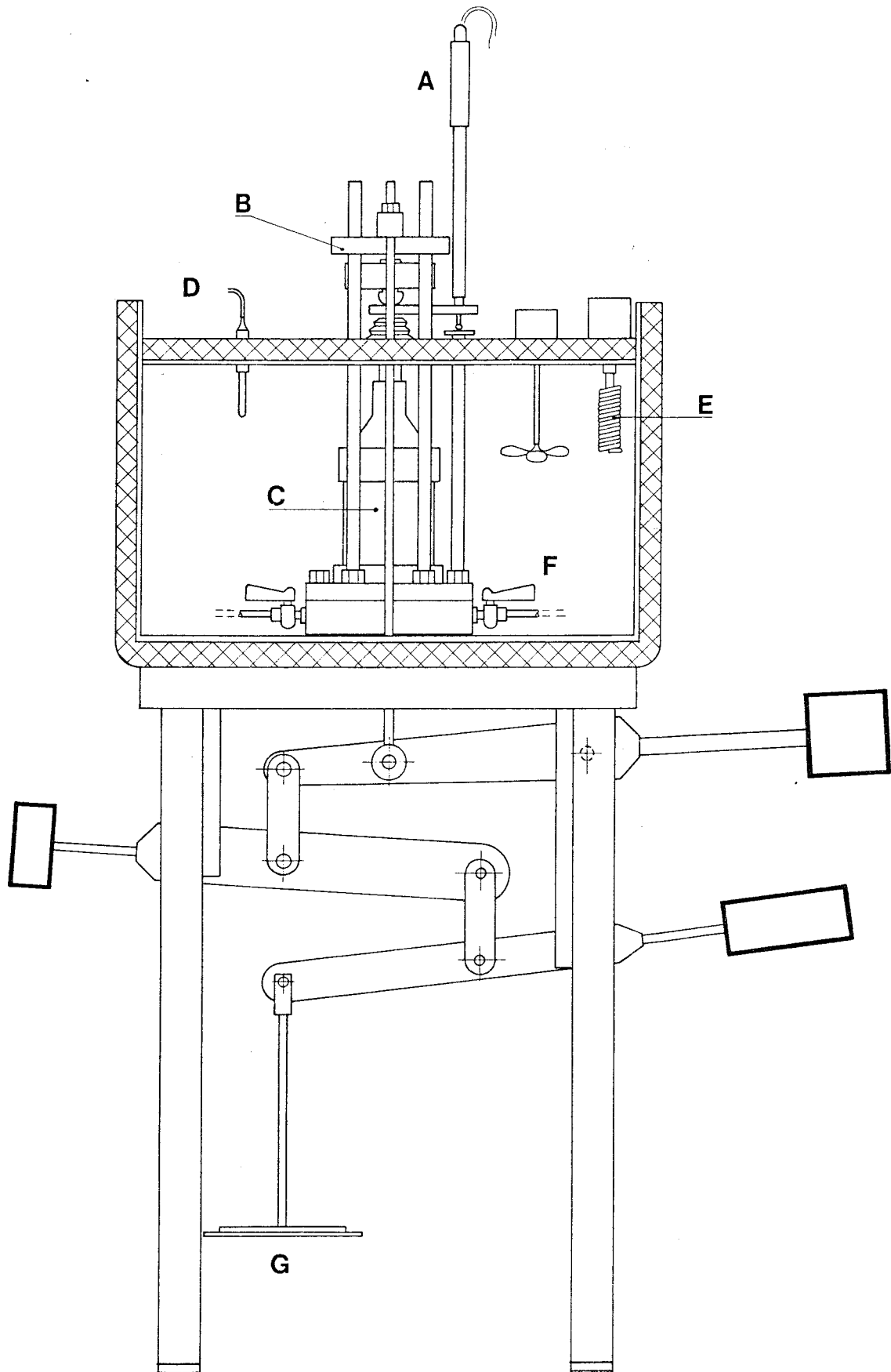


Fig.13. The constant stress device for creep testing.

A) Electronic strain gauge, B) Yoke for axial load transfer, C) Triaxial cell, D) Thermostat, E) Heater, F) Hot bath in insulated box for creep tests at elevated temperature, G) Load plate.

2.3.5 Results

Fig.14 shows a plot of the undrained creep tests which all exhibit the same characteristic retardation of the strain rate as the previously discussed illitic clays, i.e. in principle according to the general creep law of Eq.8. We see, however, that the samples with the lowest deviator stress have curve shapes indicating high $t_0:s$, which is in agreement with the prediction here that they should suffer little structural damage and behave fluid-like. As to the sample with the very high deviator stress 2500 kPa, there is some doubt concerning its relevance since this test was meant to be a single exploratory study. Assuming it to be representative of the behavior of dense bentonite at very high shear stresses, it must be concluded that the retardation of the strain rate is very moderate and that creep failure may have followed if the test had continued. This was the only case which gave such indications, although the test conditions - in contrast to those in the field - certainly offered a possibility of a fully developed failure in all the tests.

It is a wellknown fact that creep tests of illitic clay under undrained conditions tend to yield failure at shear stresses well below the conventionally determined shear strength (Fig.15), which is generally explained by the accumulated structural damage when a critical strain has been reached. The present results indicate a basic difference between illitic and (dense) smectitic clays, probably due the very strong thixotropy of the last-mentioned, which yields substantial healing effects (11,12).

Fig.16 illustrates the creep behavior of the drained samples, one of them being heated to 93 °C. The non-heated, drained samples exhibit faster creep than the undrained ones, but the tendency seems to be that they will join at the high t -values we consider in the practical application. As to the heated sample, the creep rate is approximately 3 to 6 times higher than that of the corresponding sample which was not heated. The practical consequence of this will be discussed later.

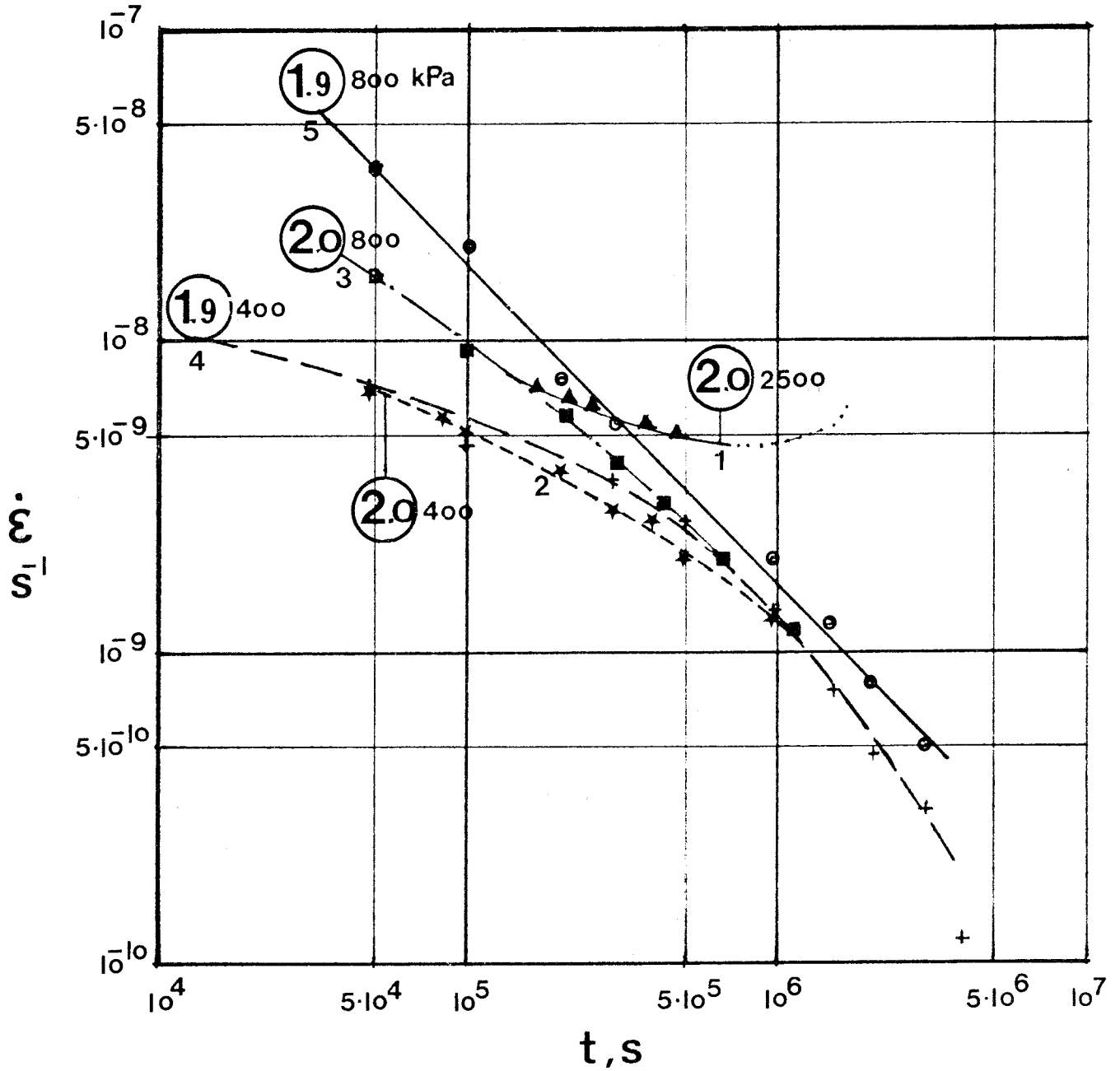


Fig.14. Creep curves of undrained MX-80 samples. Bulk densities in t/m^3 are encircled; 400 kPa etc is the "instantly" applied deviator stress; Figures 1,2,3 etc refer to the test code numbers in Table 1.

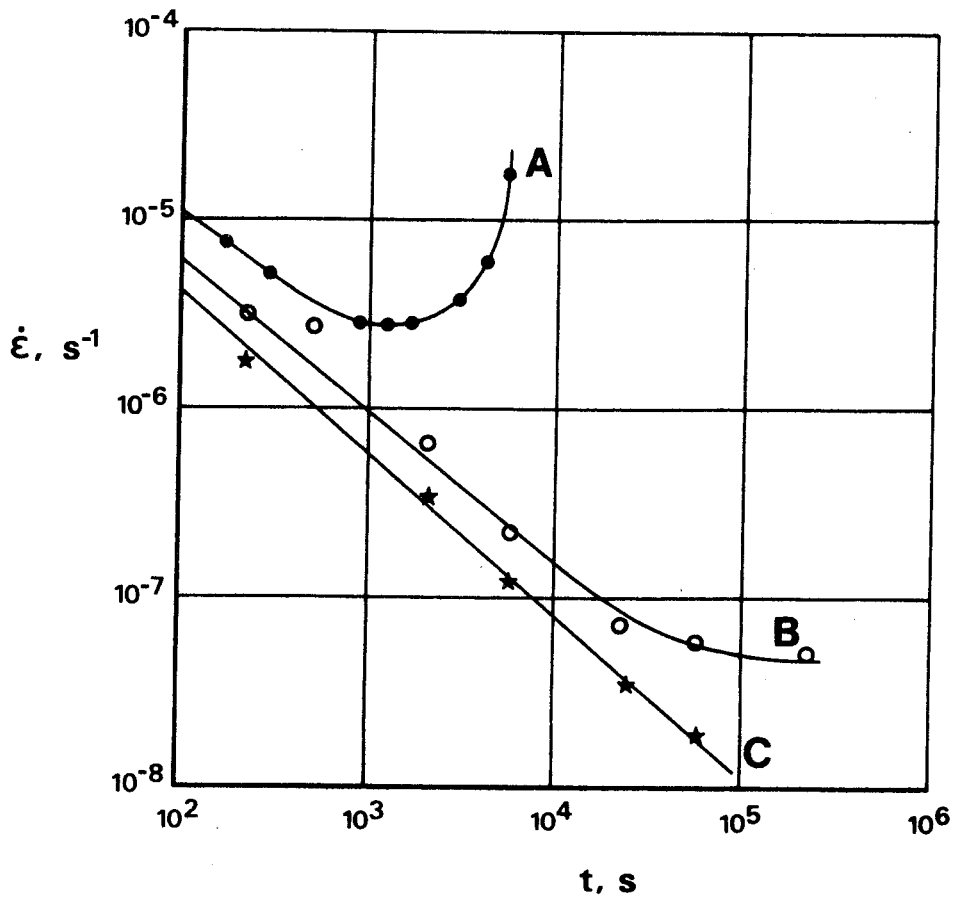


Fig.15.
 Typical set of creep curves for illitic clay. A, B, and C represent 90,85, and 70% of the maximum deviator, respectively.

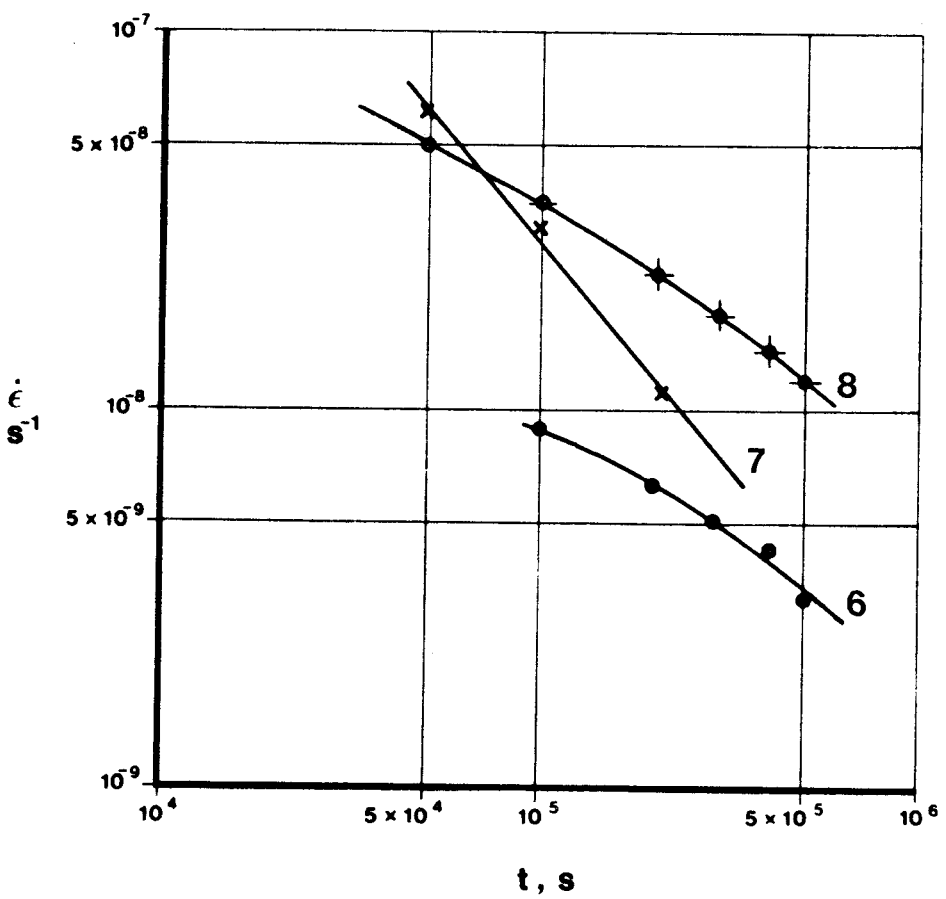


Fig.16.
 Creep curves of drained MX-80 samples. Figures refer to test code numbers in Table 1.

It should be mentioned that the pore water pressure could not be measured in all the undrained creep tests due to unexpected, repeated breakdown of the pressure gauges. Where the pressure could be properly recorded, it was found to increase successively as is usually observed in creep tests of illitic clays. As in such clays, the increased pressure in the bentonite probably reflects structural breakdown, which thus supports the previous conclusion that even matured bentonite is characterized by a certain degree of aggregation. In test no.4, for instance, the pore water pressure rose from about 40 kPa immediately after the onset of creep to a final, constant value of about 110 kPa. The cell pressure was 1.7 Mpa in all the tests with 1.9 t/m³ samples, while it was 4.6 MPa for the 2.0 t/m³ samples.

The maximum shear resistance is a function of the strain rate. Creep test no.1 indicates that a deviator stress of 2.5 Mpa may represent the maximum shear resistance at very low strain rates, but current testing actually suggests that the maximum stress is lower, even at rapid shear. General information on the stress/strain behavior is offered by the "hot" creep test (no.8) where the creep at 400 kPa deviator stress was observed for a week and where successive load steps were then applied, each with a duration of about 8 hours. The accumulated strain for each stress set is plotted in Fig.17, from which it is concluded that dense bentonite exhibits strong work-hardening, but also that the deformation modulus drops from an initial, relatively high value to a substantially lower value when the strain exceeds about 2 %. This alteration is very probably associated with a comprehensive microstructural breakdown. The major part of the strain is due to creep but the strain recording actually permits evaluation of the "initial", elastic strain which is required for the derivation of the modulus of elasticity as will be shown later in the text.

At the termination of creep test no.8, the largely distorted sample exhibited a fracture pattern which is typical for undrained shear failure, i.e. sets of perpendicular macroscopic slip planes traverse the sample (Fig.18).

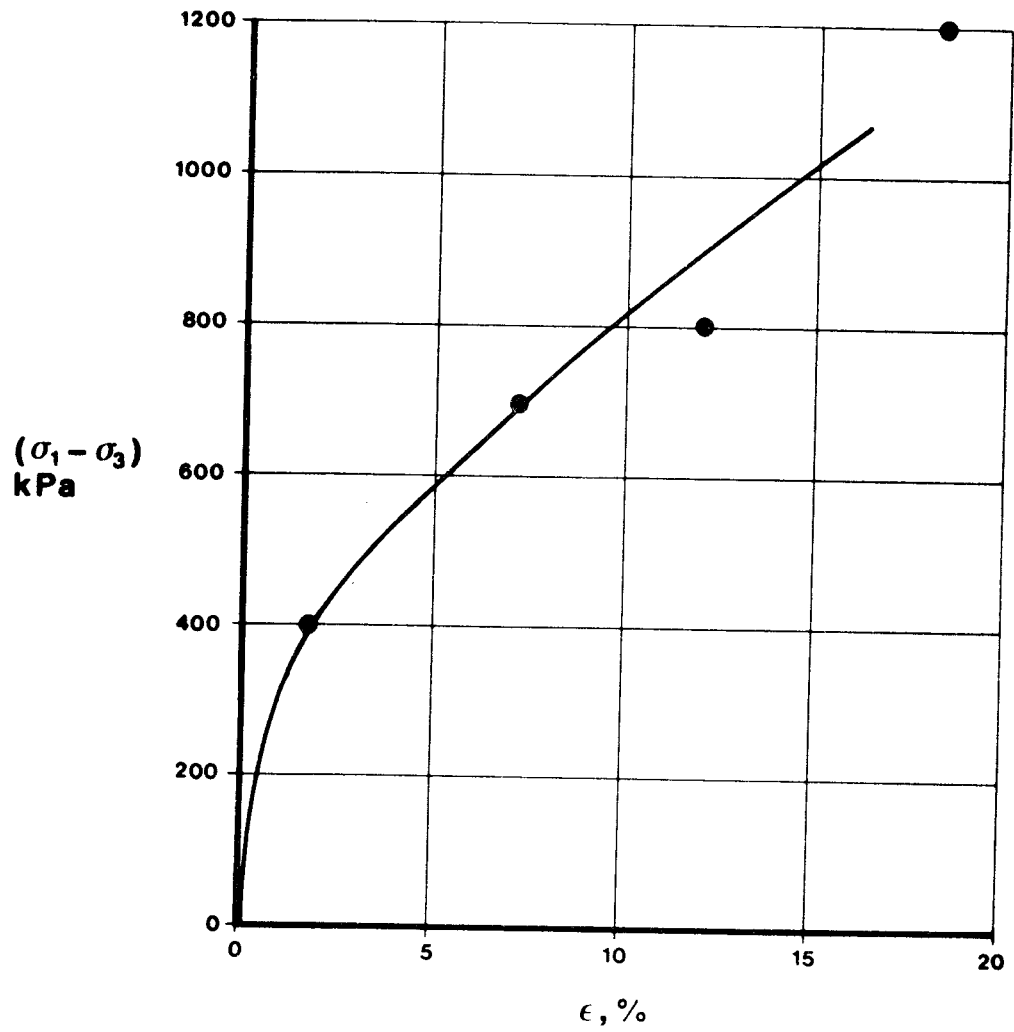


Fig.17. Plotting of deviator stress versus axial compression. Creep test no.8.

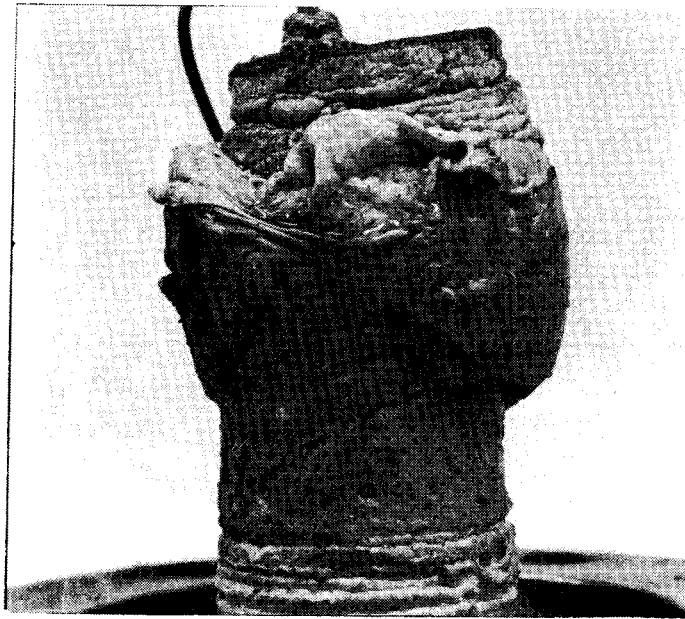


Fig.18. Appearance of creep-tested sample with final axial compression of more than 20 %.

2.4 Further aspects of the creep equation

2.4.1 General

The extrapolation of the creep strain over the rather extreme period of time considered in the KBS concepts (10^6 years), based on short term laboratory-derived parameter values, cannot be expected to yield an exact, ultimate creep settlement. It is possible, however, to identify the maximum upper limit of the canister settlement if the creep law can be proved to be valid for this clay. This does not only imply that the law can be derived theoretically, as in the present case, but also that the basic physical assumptions are correct. This brings us back to the point of mineral lattice hydration, or more precisely, to the question of the physical state of the interlayer water, which should be a determinant of the physical properties if our physical model is valid. At present, only preliminary results are available from the current research, but some of them are considered to be rather interesting and are therefore briefly reported here.

2.4.2 Evaluation of the major type of interparticle bonds from creep tests

Following FELTHAM (13) the activation energy of the dominant rate process in creep of most materials can be written as:

$$u^* = u_0 - v \cdot \tau = m k T \quad (9)$$

where u^* = the thermally accessible barrier height
 u_0 = the strength of the major type of bonds
 v = activation volume (volume of flow unit)
 τ = the applied shear stress
 m = 28 (3)
 k = Boltzmann's constant

During creep, $v \cdot \tau$ will change as a function of time. From the creep equation:

$$\dot{\epsilon} = A \cdot e^{-\frac{u_0 - v\tau}{kT}} \quad (10)$$

which applies to short time intervals, we have for approximately constant v :

$$v = kT \frac{\partial \ln \dot{\epsilon}}{\partial \tau} \quad (11)$$

This yields, for two arbitrary stress/strain sets:

$$v\tau = kT \left(\ln \frac{\dot{\epsilon}_2}{\dot{\epsilon}_1} / \ln \frac{\tau_2}{\tau_1} \right) \quad (12)$$

Considering the MX-80 clay we see that when t exceeds about $5 \cdot 10^5$ s, the creep rate is approximately proportional to the applied stress, i.e. the expression within the parenthesis of Eq.12 equals unity. In earlier stages this value is higher; for $t=5 \cdot 10^4$ s it is about 2.3 for the low bulk density 1.9 t/m^3 and 1.3 for 2 t/m^3 . Using Eq.9 we find that the left membrum of Eq.12 is small compared to mkT , and that u_0 is approximately 0.6 eV. This value is within the upper range of the hydrogen bond strength spectrum, which therefore supports the belief that water lattices are largely responsible for the physical behavior of the investigated smectite clay.

If the same evaluation is made of creep curves for aggregated illitic clays, higher bond strength values are arrived at, which illustrates that such clays gain additional shear resistance from other sources, such as mechanical interaction of neighbouring silt grains and directly contacting illite crystallites.

It must be pointed out here that although the theoretical model is correct in principle, it is rather crude. Further refinement is under way.

2.4.3 Evaluation of the physical state of interlayer water

The basic idea of this approach is that flow is equivalent to stress relaxation. For liquids, the problem of evaluating their flow properties in terms of viscosity, for instance, is that of measuring molecular mobility, which can be made by determining the duration of molecular orientation in a magnetic field as in the nuclear resonance technique (NMR). The major relevant parameter is the spin-spin coherence time T_2 for protons. It is very short for lattice protons (OH) and for strongly mineral-adsorbed water molecules, while it is long for free water.

Thixotropic strength regain after remolding of clays, involving water lattice reorganization among several processes, has been investigated earlier by applying this technique (15). The present study, run by Torbjörn Carlsson at the Dept. of Physical Chemistry, KTH, is part of a research project sponsored by SKBF/KBS.

As expected, it has been found that T_2 is very short for the water content interval 25 - 35 % that is relevant to the KBS concepts (Fig.19), which points to highly ordered, "strong" water lattices. Attempts have been made to express T_2 in terms of an average activation energy for flow using the Arrhenius equation, the results pointing to values well within the range of the hydrogen bond. The influence of paramagnetic effects and other disturbances have not been completely mapped yet, however, and no safe conclusions can be drawn so far.

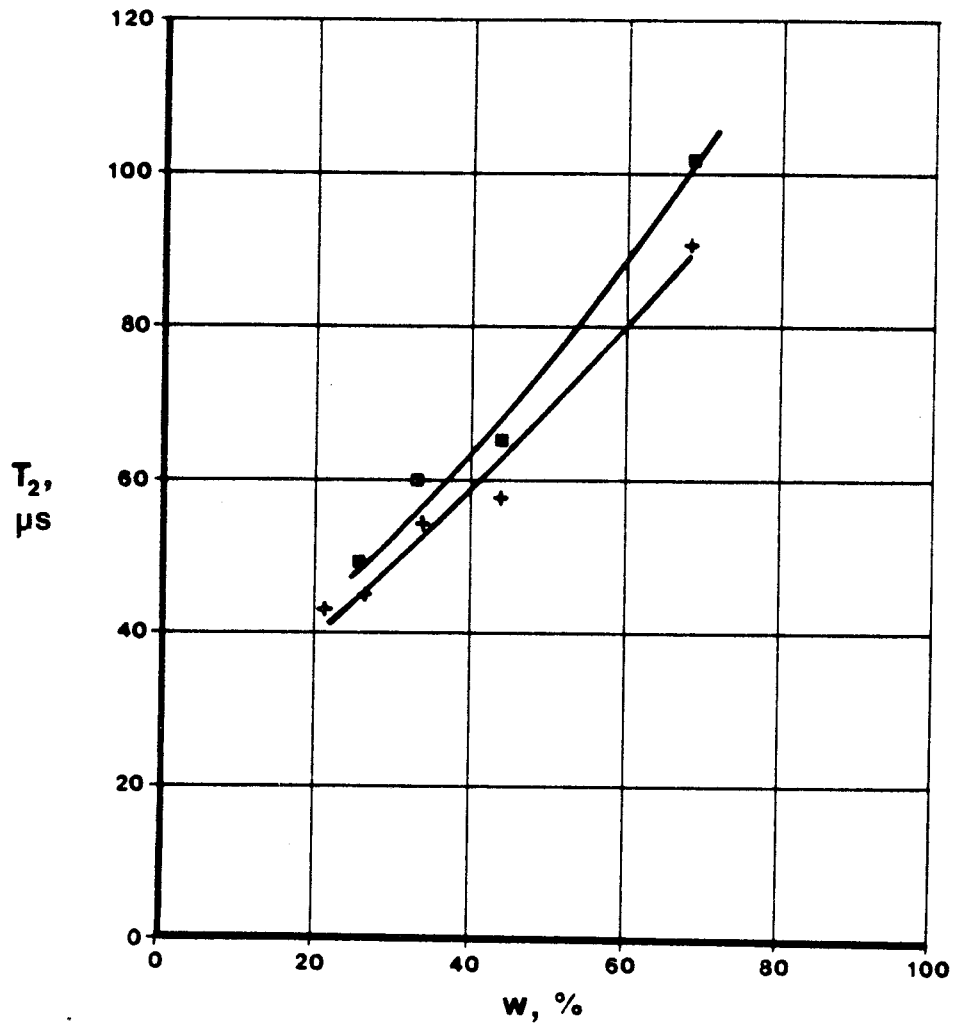


Fig.19. Spin-spin coherence time T_2 as a function of the water content of MX-80 bentonite with a bulk density ranging from about 1.6 to 2.1 t/m³. Upper curve represents 25 °C and the lower 10 °C (T.Carlsson).

2.5 Constitutive relationships of highly compacted bentonite

2.5.1 Object

The practical applications that we are concerned with require the definition of a complete creep law with respect to the influence of the deviator stress and of heating. Also, the rock displacement case requires the definition and setting of suitable parameters for the stress/strain relationship at rapid, induced shear.

As to the creep, the theoretical as well as the experimental basis is sufficient to make the creep law complete. For the other case, which is actually very complex, different approaches can be made, the simplest but least correct one being based on linear elastic analysis. It is conservative under certain circumstances and will be the only treatment presented in this report. For a more relevant approach, the real non-linear behavior of the various components (cf. Fig.2) needs to be taken into account; such a development is under way and will be presented later.

2.5.2 The complete creep equation

The outcome of the theoretical considerations and the bentonite creep tests, is that the average creep strain rate at room temperature can be expressed by use of Eq.8. Attempts have been made to extend the relationship to cover the influence of stress as well as temperature and they have led to Eq.13 for low and intermediate stresses and very moderate temperatures (3):

$$\dot{\epsilon} = \beta TD \frac{1}{t+t_0} \quad (13)$$

where β = constant

T = absolute temperature

D = deviator stress

The influence of stress is reasonably well accounted for by this equation, while the effect of heating is largely underestimated. Thus, the temperature of tests no.1 - 7 was 295 K and 366 K of test no.8, which would only yield a 25 % higher creep rate of the latter according to the equation, while it actually increased 3 to 6 times.

Although only one creep test has been run at elevated temperature so far, the observed strong influence of heating is very probably representative. Thus, earlier tests on illitic clay (16) have shown that the creep rate is increased almost linearly by 2.3 times when the temperature is raised from 24 °C to 60°C (Fig.20), which suggests that a temperature raise from 22 °C to 93 °C would have increased the creep rate of the illitic clay by almost 5 times.

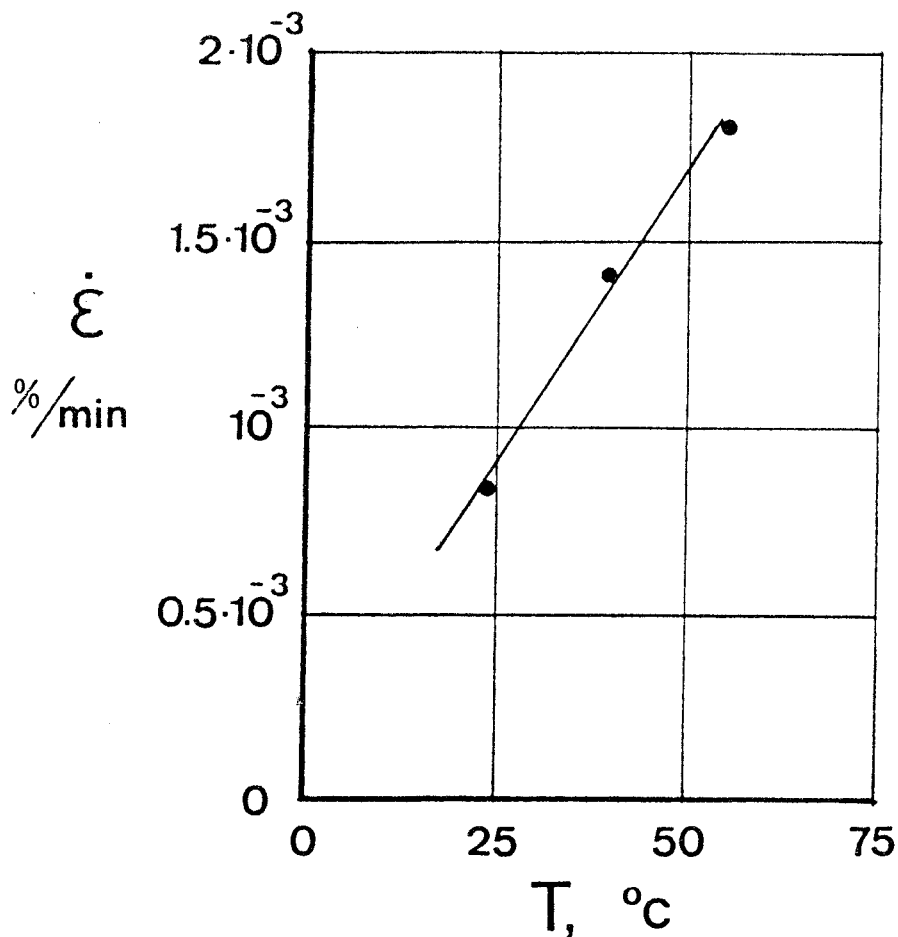


Fig.20 . Influence of temperature on the creep rate of soft illitic clay (16).

Considering the rather extreme period of time for which the creep settlement should be predicted, t_0 can be omitted. Then, the constant of Eq.13 remains to be determined and for this purpose a low stress test series should form the basis of its evaluation, simply because the deviators in the clay mass will actually be very low. A low density test series should in fact also be used, since a "worst case" scenario may actually involve a reduction of the bulk density to about 1.9 t/m^3 (17). These criteria are reasonably well fulfilled by the undrained creep test of the 1.9 t/m^3 sample with 400 kPa deviator stress and $T = 295 \text{ K}$. The evaluated constant turned out to be $3.6 \cdot 10^{-9}$, and the final form of the creep strain equation:

$$\begin{aligned} \epsilon &= \beta TD \ln t & (14) \\ & (t \gg 0 \text{ s}) \end{aligned}$$

The given figure for the constant is valid on the condition that the deviator D is expressed in kPa, that the temperature T is expressed in Kelvins and that it is not very different from room temperature, and that the time t after onset of the creep is expressed in seconds. Also, it is representative of water saturated Na bentonite with a bulk density of 1.9 t/m^3 .

2.5.3 Stress/strain relationships for the rock shear case

"Instantaneous" or rapid rock displacement according to Fig.2 certainly yields local shear failure along the displaced rock/clay interface. Sufficiently small displacements confine this overstressing to a narrow zone, leaving the rest of the clay mass in pseudo-elastic state. The stress state of the canister, which is rather stiff in comparison with the clay, is very much dependent on the stress/strain behavior of the clay, which requires evaluation of its modulus of elasticity for computational treatment. This parameter can be estimated from the initial branch of the creep curves, but for this purpose we need to consider the delay in load transfer to the samples that was caused by the inertia of the lever system of the loading device. The delay, which was measured by use of a metal dummy equipped with a load cell, means, for instance, that only 29 % of the nominal, "applied" stress actually affects the loaded sample after 60 seconds. After 1000 seconds this percentage is 60, and after 2700 seconds 72.

Considering the associated stress reduction, the E-modulus has been evaluated from the non-heated creep tests (Table 2). The interpretation was based on the conservative estimation that the stress was constant from the moment of load application to the time when the first recording took place, i.e. after 60 - 2700 seconds.

Table 2. The modulus of elasticity as interpreted from the creep tests

Bulk density t/m^3	Nominal deviator kPa	Actual deviator kPa	E-modulus MPa
2.0	1600	460	117
2.0	800	480	369
2.0	400	290	533
1.9	800	230	41
1.9	400	115	46
1.9	400	115	31

The actual bulk density of the bentonite clay in the deposition holes will be in the interval 2.0 - 2.1 t/m³, which would yield a slightly higher E-modulus than the average value 340 MPa for the 2.0 t/m³ samples in Table 2. Since this value is based on conservative estimates it should be approximately valid also for the slightly higher bulk density which is expected for the clay embedding the canisters. This would be in good agreement with an earlier determination of the E-modulus of highly compacted, non-saturated bentonite by rapid, uniaxial compression at a constant strain rate (18). This determination gave E = 270 MPa and a shear strength of slightly more than 8 MPa of a 2.05 t/m³ MX-80 sample with about 50 % degree of water saturation. It was concluded that these figures are expected to drop when the bentonite becomes saturated, which suggests that the 340 MPa value is an overestimation and that E = 200 MPa is a more plausible value. Actually, recent checking by uniaxial, compression with a strain rate of 1 % per minute of a 2.0 t/m³ sample, yielded a shear strength of 1.1 MPa and an E-modulus, evaluated from the straight portion of the stress/strain curve, of slightly more than 100 MPa.

3. SETTLEMENT OF CANISTERS - 1:st APPLICATION

3.1 Definition

Strictly speaking, the settlement is not only caused by shear-induced creep; there is also an elastic displacement, which is developed at the load application. In practice, this elastic part is associated with the deposition of the canisters in the deposition holes, i.e. when the bentonite is not yet water saturated. It is of the order of a few millimeters and is followed by creep under practically constant volume conditions, first of the non-saturated material, and then of the saturated and matured bentonite. The major part of the creep strain will be that of the saturated and matured clay, which can be reasonably well predicted by use of the derived creep equation.

The basis of the settlement calculation is the geometry shown in Fig.21. The weight of the canisters will produce a vertical pressure on the clay of 400 kPa at maximum. The creep parameters valid for a bulk density of 1.9 t/m^3 and room temperature were applied.

3.2 Calculation

The calculation of the creep settlement, which is an axi-symmetric problem, was performed by the Computational Mechanics Centre (CMC)*, Southampton, England, by applying boundary element analysis. BEM offers certain advantages over "domain" type solutions, such as finite element analysis. Thus, the systems of generated equations is small and it is well suited to stress analyses.

The applied boundary element mesh is shown in Fig.22. The crosses below the base of the canister mark the points for which the principal stresses were determined. Two different conditions were considered: that of slip between the clay and the rock and between

* Drs. C.A.Brebbia and D.Danson.

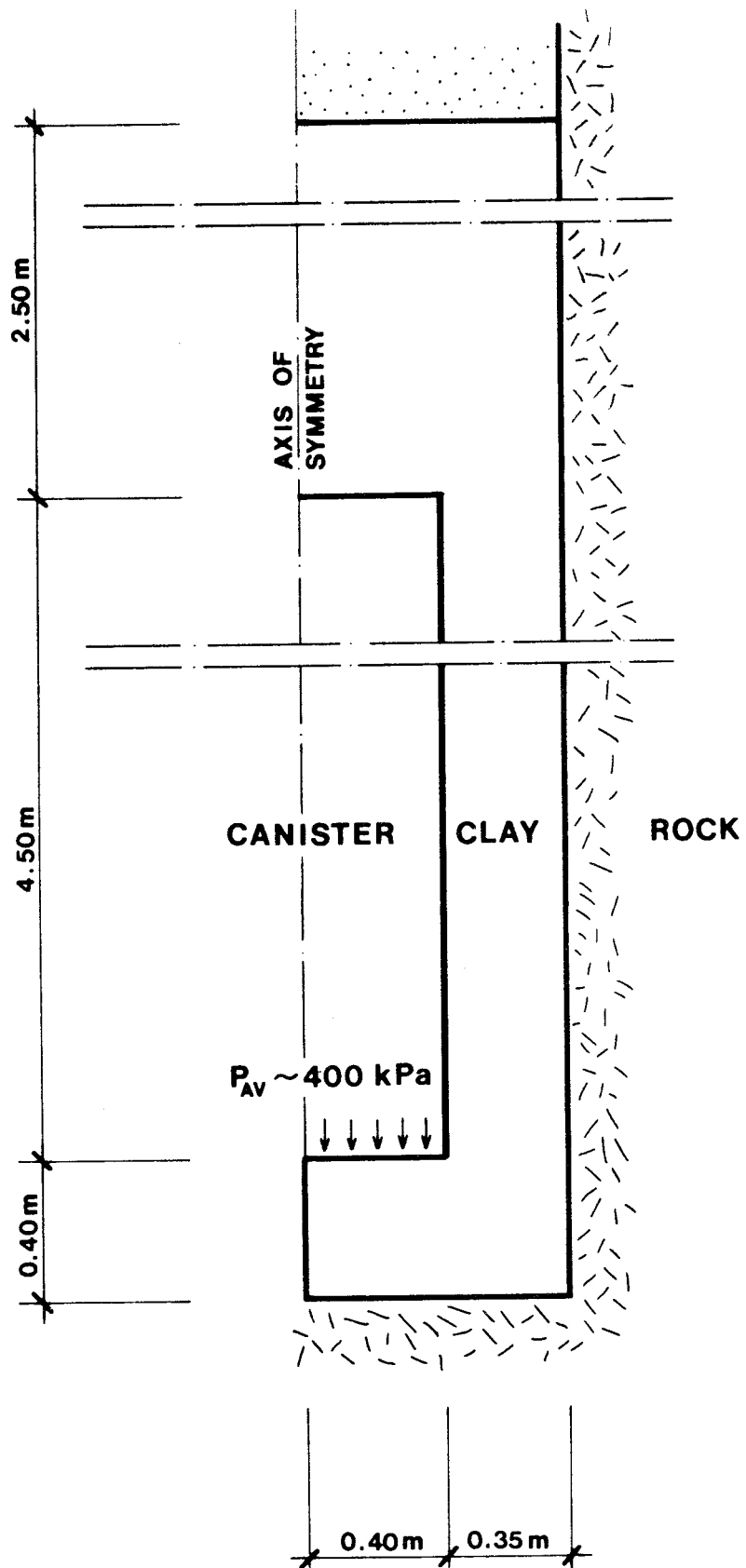


Fig.21. The considered case of canister settlement.

the clay and the cylinder, and that of no slip at these positions.

The outcome of the calculation, which is given as an appendix, is that the creep settlement in one million years will be very small,

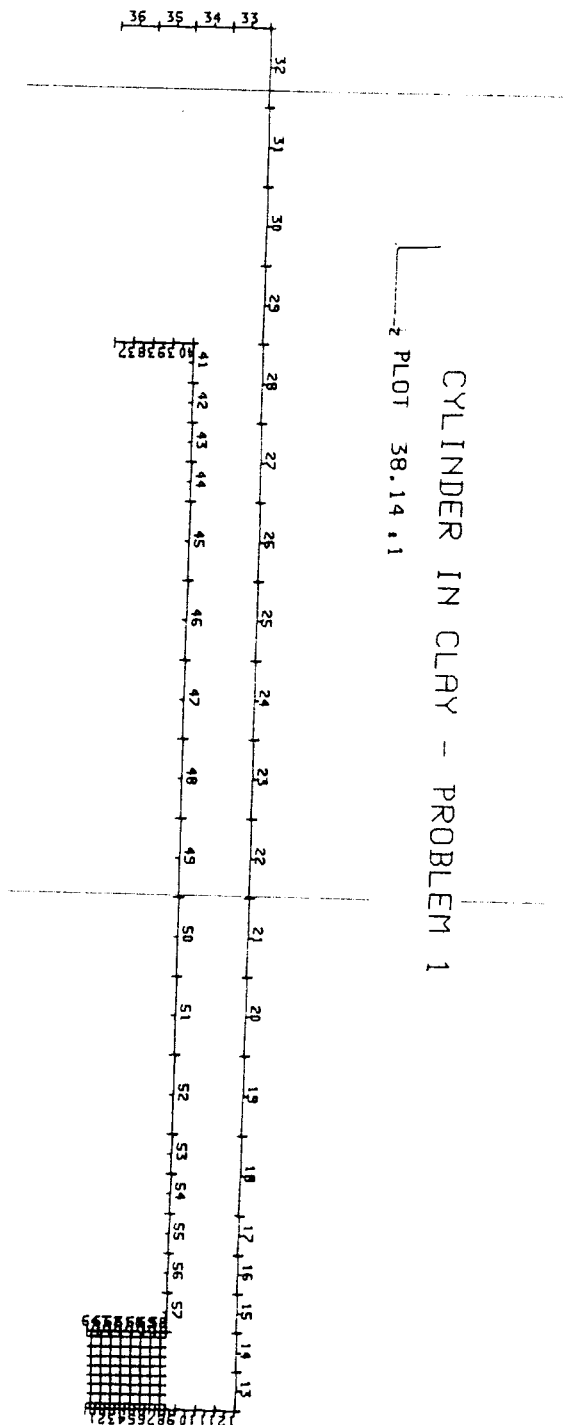


Fig.22. The boundary element mesh (CMC).

i.e. a few millimeters (Table 3). The application of the low-temperature version of the creep formula Eq.14, implies that the temperature is kept constant at 22 C° throughout the considered period of time. However, the average temperature will range between 315 and 335 K for several thousand years, which increases the creep rate by 2 - 3 times during this time interval. The heating takes place early in the creep evolution, which yields a net settlement after one million years of 10 mm at maximum.

Table 3. Settlement versus time (CMC)

Time, years	Settlement, mm	
	Slip case	Non-slip case
1	0.76	1.06
10	0.86	1.30
10 ²	0.97	1.45
10 ³	1.07	1.61
10 ⁴	1.17	1.76
10 ⁵	1.27	1.91
10 ⁶	1.37	2.07

4. ROCK SHEAR DISPLACEMENT - 2:ND APPLICATION4.1 Definition, pilot studies

A first approach has been made to solve the computational problem of rock shear displacement by applying 2 and 3 D linear elastic analyses, and a 2 D elasto-plastic analysis as well (Fig.23).

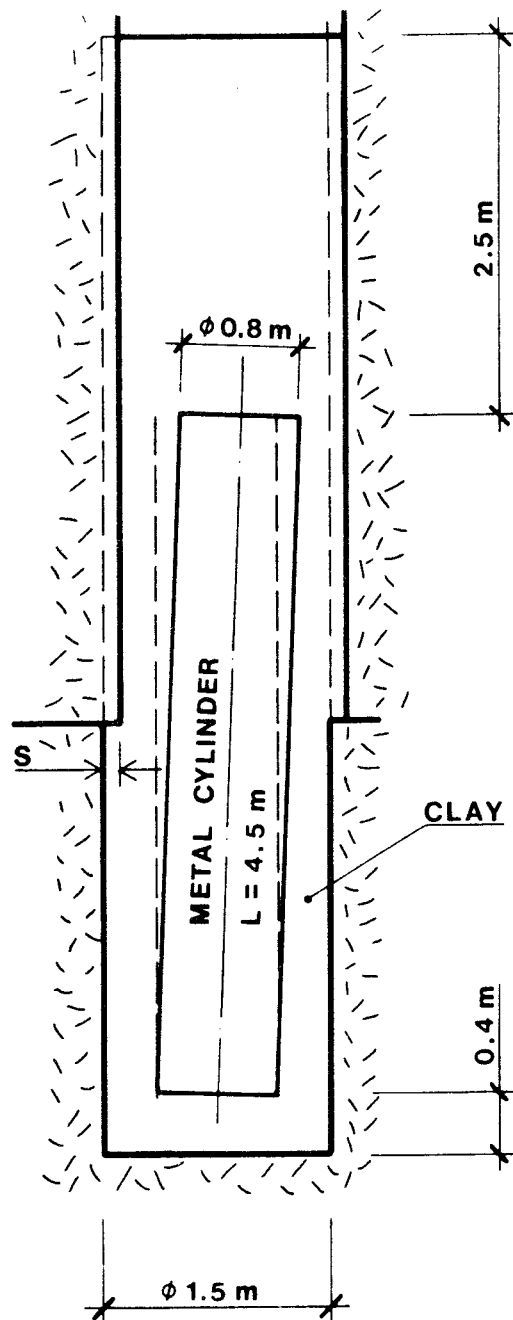


Fig.23. The considered case of rock shear.

The 3 D analysis, which was performed by Dr Fred Nilsson (19), showed that a non-symmetrical shear yields the highest moment in the cylinder. Using this constellation and the E-moduli $6 \cdot 10^3$ MPa for the bentonite and $1.33 \cdot 10^5$ MPa for the copper canister, and Poisson's ratio 0.45 for the bentonite and 0.35 for the copper, he calculated the stresses induced by a rapid 1 cm rock displacement. As shown earlier in the present report, the actual E-modulus of the bentonite turns out to be much lower, and a more realistic study, based on E-moduli in the range of 200 - 1000 MPa, is presently under way.

The outcome of Nilsson's analysis was that the axial stress component was completely dominating, and that its maximum value in the copper canisters was about 375 MPa in tension and compression. In the plane of shear local stress concentrations were recorded. The tension stress is beyond the elastic stress/strain region of copper which means that the canisters become deformed sufficiently much to require that the non-linear stress/strain behavior of copper as well of bentonite be considered.

A preliminary 2 D calculation with $E = 200$ MPa and with the criterion that plastic conditions appear in the bentonite when the shear stress equals 8 MPa, has been run by Dr Kenneth Axelsson (20). Applying the afore-mentioned non-symmetrical shear conditions, and the same copper material properties as in the 3 D analysis, the elasto-plastic approach yielded a maximum tension stress in the copper of about 20 MPa, which is well below the yield stress of this material. All these calculations were made by applying finite element analysis.

5. CONCLUSIONS

The physico/mechanical behavior of highly compacted bentonite is governed by the strongly hydrophilic character of its smectite components, in the sense that the adsorbed water is a determinant of its bulk behavior. This yields very obvious thixotropic and viscous properties, the latter being manifested by creep strain rates that are of the same order of magnitude as those of much softer illitic clays. It is concluded, however, that the stress/strain/time parameters used in applied material sciences, including soil mechanics, can be sufficiently well defined and determined also for highly compacted bentonite. This enables us to make reliable settlement calculations as well as stress/strain analyses of processes which involve extension into the plastic region.

As to settlement calculations, all necessary basic clay data are at hand and the analysis presented in this report is sufficiently rigorous for practical purposes. Concerning the rock shear case, the pilot studies show that a closer analysis, with due respect to the non-linear behavior of the involved materials, is required to fully understand the impact of rock displacements on the physical state of the metal cylinders. This also calls for an extended study of the physical background of the visco/elasto/plastic nature of the clay material.

At present, it seems as if a rapid rock displacement of at least 1 cm can take place without harming the canisters.

6. ACKNOWLEDGEMENTS

The author wishes to express his sincere gratitude to Professor Paul Feltham, Dept. of Physics, Brunel University, England, who outlined the basis of the creep philosophy and theory for evaluation of activation energies for molecular slip.

Also, the author is very much indebted to Dr. Lennart Börgesson, Mr. Sven Knutsson, Mr. Ulf Stenman, and Mr. Ulf Sundström, all at the Division of Soil Mechanics, University of Luleå. Mr. Knutsson designed the loading device and arranged the high-pressure triaxial equipment, while Mr. Stenman and Mr. Sundström ran the experiments and helped to arrange the recording. Dr. Börgesson was in charge of the laboratory work and he also contributed to the evaluation of the tests.

7. REFERENCES

1. FORSLIND, E. & JACOBSSON, A. Clay/water interactions. Final Technical Report. European Research Office, United States Army, Contract No. DAJA 37-72-C-3894, 1973.
2. EDELMAN, C.H. & FAVEJEE, J.CH.L. On the structure of montmorillonite and halloysite. Zeitschrift für Kristallographie, Vol.102, 1943 (pp.417 - 431).
3. PUSCH, R. & FELTHAM, P. A stochastic model of the creep of soils. Géotechnique, Vol.30, No.4, 1980 (pp. 497 - 506).
4. PUSCH, R. & FELTHAM, P. Computer simulation of creep of clay. Journal of the Soil Mechanics and Foundations Division. ASCE, Vol.107, No.GT 1, Jan. 1981.
5. FELTHAM, P. A stochastic model of creep. Physica Status Solidi, Vol.30, 1968 (pp.135 - 146).
6. SINGH, A. & MITCHELL, J.K. General stress-strain function of soils. Journal of the Soil Mechanics and Foundations Division. ASCE, Vol.94, No.SM 1, 1968 (pp.21 - 46).
7. PUSCH, R. Mineral/water interactions and their influence on the physical behavior of highly compacted Na bentonite. Canadian Geotechnical Journal, Vol.19, No.3, 1982 (pp.381 - 387).

8. PUSCH,R. Water uptake, migration, and swelling characteristics of unsaturated and saturated, highly compacted bentonite. SKBF/KBS Teknisk Rapport 80-11, 1980.
9. PUSCH,R., BÖRGE-SSON,L. & NILSSON,J. "Buffer Mass Test - Buffer Materials". Stripa Project 82-06. SKBF/KBS Internal Report, 1982.
10. ALLARD,B. Sorption of actinides in granitic rock. SKBF/KBS Teknisk Rapport 82-21, 1982.
11. PUSCH,R. Creep of soils. Ruhr-Universität Bochum, Heft 5, Serie Grundbau, Nov. 1979.
12. TING,J.M. On the nature of the minimum creep rate-time correlation for soil, ice, and frozen soil. Canadian Geotechnical Journal, Vol.20, 1983.
13. FELTHAM,P. A stochastic model of crystal plasticity.
14. FELTHAM,P. On the flow stress of metals at low temperatures. Phil. Mag., Vol.21, 1970 (p.765)
15. JACOBSSON,A. & PUSCH,R. Thixotropic action in remoulded quick clay. Bull. Internat. Assoc. Engng.Geology, No. 5, 1972 (pp. 105 - 110).
16. PUSCH,R. Inverkan av förhöjd temperatur på finkornig jord - förstudie. Statens Råd för Byggnadsforskning. Byggdok. 32401, 1979.
17. PUSCH,R. Stability of bentonite gels in crystalline rock - physical aspects. SKBF/KBS Teknisk Rapport 83-04, 1983.

18. PUSCH,R. Highly compacted Na bentonite as buffer substance. KBS Teknisk Rapport 74, 1978.
19. NILSSON,F. Linjär analys av kopparkapsel utsatt för bergförskjutning. IFM Akustikbyrån, TM 5.242, 1982.
20. AXELSSON,K. Elasto-plastisk analys av kopparkapsel utsatt för bergförskjutning. Internal Report, University of Luleå, Div. Soil Mechanics, May 25, 1982.

APPENDIX

COMPUTATIONAL MECHANICS CENTRE, "CYLINDER
IN CLAY"; BEM CALCULATION

Settlement of Cylinder in Clay

1. Incompressible Material ($\nu = 0.5$)

In theory the boundary element method is well suited to solving problems involving incompressible materials. However the axisymmetric module of BEASY cannot solve such problems for the following reasons.

The basic boundary integral expression in elasticity is

$$c(x) u_k(x) = \int_{\Gamma} U_{ki}(x,y) t_i(y) d\Gamma_y - \int_{\Gamma} T_{ki}(x,y) u_i(y) d\Gamma_y \quad (1)$$

where

$$\begin{aligned} c(x) &= 0 && x \text{ outside the domain} \\ c(x) &= \frac{1}{2} && x \text{ on smooth part of boundary } \Gamma \\ c(x) &= 1 && x \text{ inside the domain} \end{aligned}$$

$u_i(y)$ is the displacement at y

$t_i(y)$ is the traction at y

$U_{ki}(x,y)$ and $T_{ki}(x,y)$ are kernel functions which define the displacements and tractions at a point y due to a unit load at another point x .

The displacement kernels are given by

$$\begin{aligned} U_{rr} &= \frac{1}{16\pi^2 (1-\nu) \mu r \sqrt{Rr}} \left\{ (3-4\nu) Q_{\frac{1}{2}}(\gamma) + \frac{(Z-z)^2}{Rr} \frac{dQ_{\frac{1}{2}}(\gamma)}{d\gamma} \right\} \\ U_{rz} &= \frac{Z-z}{16\pi^2 (1-\nu) \mu r \sqrt{Rr}} \left\{ \frac{Q_{\frac{1}{2}}(\gamma)}{2} - \left[\gamma - \frac{r}{R} \right] \frac{dQ_{\frac{1}{2}}(\gamma)}{d\gamma} \right\} \\ U_{zr} &= - \frac{Z-z}{16\pi^2 (1-\nu) \mu r \sqrt{Rr}} \left\{ \frac{Q_{-\frac{1}{2}}(\gamma)}{2} + \left[\gamma - \frac{r}{R} \right] \frac{dQ_{-\frac{1}{2}}(\gamma)}{d\gamma} \right\} \\ U_{zz} &= \frac{1}{16\pi^2 (1-\nu) \mu r \sqrt{Rr}} \left\{ (3-4\nu) Q_{-\frac{1}{2}}(\gamma) - \frac{(Z-z)^2}{Rr} \frac{dQ_{-\frac{1}{2}}(\gamma)}{d\gamma} \right\} \end{aligned} \quad (2)$$

and the traction kernels by

$$T_{rr} = 2\mu \left[\left\{ \frac{1-\nu}{1-2\nu} \frac{\partial U_{rr}}{\partial r} + \frac{\nu}{1-2\nu} \left(\frac{U_{rr}}{r} + \frac{\partial U_{rz}}{\partial z} \right) \right\} n_r + \frac{1}{2} \left(\frac{\partial U_{rr}}{\partial z} + \frac{\partial U_{rz}}{\partial r} \right) n_z \right]$$

$$T_{rz} = 2\mu \left[\left\{ \frac{1-\nu}{1-2\nu} \frac{\partial U_{rz}}{\partial z} + \frac{\nu}{1-2\nu} \left(\frac{U_{rr}}{r} + \frac{\partial U_{rr}}{\partial r} \right) \right\} n_z + \frac{1}{2} \left(\frac{\partial U_{rr}}{\partial z} + \frac{\partial U_{rz}}{\partial r} \right) n_r \right]$$

$$T_{zr} = 2\mu \left[\left\{ \frac{1-\nu}{1-2\nu} \frac{\partial U_{zr}}{\partial r} + \frac{\nu}{1-2\nu} \left(\frac{U_{zr}}{r} + \frac{\partial U_{zz}}{\partial z} \right) \right\} n_r + \frac{1}{2} \left(\frac{\partial U_{zr}}{\partial z} + \frac{\partial U_{zz}}{\partial r} \right) n_z \right] \quad (3)$$

$$T_{zz} = 2\mu \left[\left\{ \frac{1-\nu}{1-2\nu} \frac{\partial U_{zz}}{\partial z} + \frac{\nu}{1-2\nu} \left(\frac{U_{zr}}{r} + \frac{\partial U_{zr}}{\partial r} \right) \right\} n_z + \frac{1}{2} \left(\frac{\partial U_{zr}}{\partial z} + \frac{\partial U_{zz}}{\partial r} \right) n_r \right]$$

where μ is the shear modulus

ν is Poisson's ratio

R is the r -coordinate of the point x

Z is the z -coordinate of the point x

r is the r -coordinate of the point y

z is the z -coordinate of the point y

$$\gamma = 1 + \frac{(Z-z)^2 + (R-r)^2}{2Rr}$$

$Q_{-\frac{1}{2}}(\gamma)$, $Q_{\frac{1}{2}}(\gamma)$ are Legendre functions of the second kind.

n_r , n_z are the r and z -components respectively of the unit outward normal to the boundary at the point y .

Substitution of Equations (2) into Equations (3) would, no doubt, eliminate the $(1-2\nu)$ from the denominator of Equations (3). However this was not done owing to tedious algebra required to do it and Equations (3) were programmed as they stand.

±

2. Calculation of the Deviator Stress D

In the telex from Dr. Pusch dated 21st December 1983 it was stated that $\sigma_2 = \sigma_3$.

In a subsequent phone call with Mr. Danson σ_1 , σ_2 and σ_3 were defined by Dr. Pusch as follows.

σ_1 : The larger (i.e. more positive) of the principal stresses in the rz-plane

σ_2 : The smaller (i.e. more negative) of the principal stresses in the rz-plane

σ_3 : The hoop stress

With these definitions, and with nature of the loading on the clay σ_2 is not equal to σ_3 . Dr. Pusch said that the hoop stress σ_3 could be ignored and that the deviator D should be defined as

$$D = \sigma_1 - \sigma_2 \quad (4)$$

3. Calculation of Settlement of the Cylinder

The axial strain for the clay is given by

$$\epsilon = D\beta T \ln(t + t_0) \quad (5)$$

The settlement Δ was obtained by integrating this axial strain from the bed rock to the base of the cylinder. Thus

$$\Delta = \int_{\ell} D \, d\ell \, \beta T \ln(t + t_0) \quad (6)$$

Equation (6) will produce a different result depending on which path ℓ is taken. The result will be quite different if ℓ is taken under the axis of the cylinder than if ℓ is taken under the edge of the cylinder. The reason for this is that the strain field described by ℓ is incompatible with the theory of elasticity used to calculate D. To resolve this problem an

average settlement was calculated by integrating Equation (6) over the base of the cylinder and dividing by its area. Thus,

$$\Delta_{av} = \frac{1}{A} \int_A \int_{\ell} D \, d\ell \, dA \, \beta T \ln(t+t_0) \quad (7)$$

$$\Delta_{av} = \frac{1}{A} \int_V D \, dv \, \beta T \ln(t+t_0) \quad (8)$$

where A is the area of the base of the cylinder.

4. Numerical Calculation

In order to evaluate $\int_V D \, dv$ 64 internal points were placed under the cylinder. A short program was written to take the output from a BEASY run, calculate the principal stresses and the deviator, and integrate the deviator over the volume.

Two different types of boundary conditions were tried. The first allowed sliding between the clay and the base of the cylinder and between the clay and the bed rock and the second assumed no slip at these positions. These boundary conditions were thought to represent the extreme cases.

For the sliding case we obtained the result

$$\int_v D dv = 27.06 \text{ kPa} \quad (9)$$

and for the no slip case we obtained the result

$$\int_v D dv = 43.05 \text{ kPa} \quad (10)$$

Putting Equations (9) and (10) into Equation (8) substituting the appropriate numerical values for βT and t_0 we get for the sliding case

$$\Delta_{av} = 0.0441 \ln \{(31.56t + 0.1) \times 10^6\} \text{ mm} \quad (10)$$

and for the no slip case

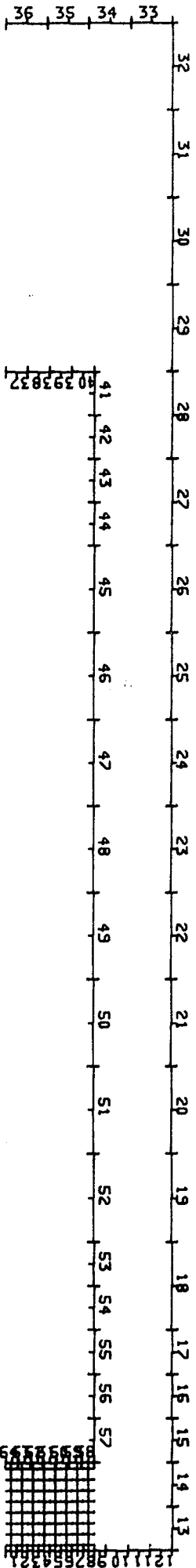
$$\Delta_{av} = 0.0702 \ln \{(31.56t + 0.1) \times 10^6\} \text{ mm} \quad (11)$$

where t is measured in years in Equations (10) and (11).

These equations are evaluated in Table 1.

Settlement mm		
Time Years	Sliding case	No slip case
1	0.762	1.061
10	0.863	1.300
100	0.965	1.453
1,000	1.066	1.606
10,000	1.168	1.759
100,000	1.269	1.912
1,000,000	1.371	2.065

Table 1 Settlement of Cylinder



CYLINDER IN CLY - PROBLEM 1

- P I N T 38.14.1

LIST OF KBS's TECHNICAL REPORTS

1977-78

TR 121 KBS Technical Reports 1 - 120.
Summaries. Stockholm, May 1979.

1979

TR 79-28 The KBS Annual Report 1979.
KBS Technical Reports 79-01--79-27.
Summaries. Stockholm, March 1980.

1980

TR 80-26 The KBS Annual Report 1980.
KBS Technical Reports 80-01--80-25.
Summaries. Stockholm, March 1981.

1981

TR 81-17 The KBS Annual Report 1981.
KBS Technical Reports 81-01--81-16
Summaries. Stockholm, April 1982.

1983

TR 83-01 Radionuclide transport in a single fissure
A laboratory study
Trygve E Eriksen
Department of Nuclear Chemistry
The Royal Institute of Technology
Stockholm, Sweden 1983-01-19

TR 83-02 The possible effects of alfa and beta radiolysis
on the matrix dissolution of spent nuclear fuel
I Grenthe
I Puigdomènech
J Bruno
Department of Inorganic Chemistry
Royal Institute of Technology
Stockholm, Sweden January 1983

- TR 83-03 Smectite alteration
Proceedings of a colloquium at State University of
New York at Buffalo, May 26-27, 1982
Compiled by Duwayne M Anderson
State University of New York at Buffalo
February 15, 1983
- TR 83-04 Stability of bentonite gels in crystalline rock -
Physical aspects
Roland Pusch
Division Soil Mechanics, University of Luleå
Luleå, Sweden, 1983-02-20
- TR 83-05 Studies of pitting corrosion on archeological
bronzes
Åke Bresle
Jozef Saers
Birgit Arrhenius
Archeological Research Laboratory
University of Stockholm
Stockholm, Sweden 1983-02-10
- TR 83-06 Investigation of the stress corrosion cracking of
pure copper
L A Benjamin
D Hardie
R N Parkins
University of Newcastle upon Tyne
Department of Metallurgy and Engineering Materials
Newcastle upon Tyne, Great Britain, April 1983
- TR 83-07 Sorption of radionuclides on geologic media -
A literature survey. I: Fission Products
K Andersson
B Allard
Department of Nuclear Chemistry
Chalmers University of Technology
Göteborg, Sweden 1983-01-31
- TR 83-08 Formation and properties of actinide colloids
U Olofsson
B Allard
M Bengtsson
B Torstenfelt
K Andersson
Department of Nuclear Chemistry
Chalmers University of Technology
Göteborg, Sweden 1983-01-30
- TR 83-09 Complexes of actinides with naturally occurring
organic substances - Literature survey
U Olofsson
B Allard
Department of Nuclear Chemistry
Chalmers University of Technology
Göteborg, Sweden 1983-02-15
- TR 83-10 Radiolysis in nature:
Evidence from the Oklo natural reactors
David B Curtis
Alexander J Gancarz
New Mexico, USA February 1983

- TR 83-11 Description of recipient areas related to final storage of unprocessed spent nuclear fuel
Björn Sundblad
Ulla Bergström
Studsvik Energiteknik AB
Nyköping, Sweden 1983-02-07
- TR 83-12 Calculation of activity content and related properties in PWR and BWR fuel using ORIGEN 2
Ove Edlund
Studsvik Energiteknik AB
Nyköping, Sweden 1983-03-07
- TR 83-13 Sorption and diffusion studies of Cs and I in concrete
K Andersson
B Torstenfelt
B Allard
Department of Nuclear Chemistry
Chalmers University of Technology
Göteborg, Sweden 1983-01-15
- TR 83-14 The complexation of Eu(III) by fulvic acid
J A Marinsky
State University of New York at Buffalo, Buffalo, NY
1983-03-31
- TR 83-15 Diffusion measurements in crystalline rocks
Kristina Skagius
Ivars Neretnieks
Royal Institute of Technology
Stockholm, Sweden 1983-03-11
- TR 83-16 Stability of deep-sited smectite minerals in crystalline rock - chemical aspects
Roland Pusch
Division of Soil Mechanics, University of Luleå
1983-03-30
- TR 83-17 Analysis of groundwater from deep boreholes in Gideå Sif Laurent
Swedish Environmental Research Institute
Stockholm, Sweden 1983-03-09
- TR 83-18 Migration experiments in Studsvik
O Landström
Studsvik Energiteknik AB
C-E Klockars
O Persson
E-L Tullborg
S Å Larson
Swedish Geological
K Andersson
B Allard
B Torstenfelt
Chalmers University of Technology
1983-01-31

- TR 83-19 Analysis of groundwater from deep boreholes in Fjällveden
Sif Laurent
Swedish Environmental Research Institute
Stockholm, Sweden 1983-03-29
- TR 83-20 Encapsulation and handling of spent nuclear fuel for final disposal
1 Welded copper canisters
2 Pressed copper canisters (HIPOW)
3 BWR Channels in Concrete
B Lönnerberg, ASEA-ATOM
H Larker, ASEA
L Ageskog, VBB
May 1983
- TR 83-21 An analysis of the conditions of gas migration from a low-level radioactive waste repository
C Braester
Israel Institute of Technology, Haifa, Israel
R Thunvik
Royal Institute of Technology
November 1982
- TR 83-22 Calculated temperature field in and around a repository for spent nuclear fuel
Taivo Tarandi
VBB
Stockholm, Sweden April 1983
- TR 83-23
- TR 83-24 Corrosion resistance of a copper canister for spent nuclear fuel
The Swedish Corrosion Research Institute and its reference group
Stockholm, Sweden April 1983
- TR 83-25 Feasibility study of EB welding of spent nuclear fuel canisters
A Sanderson
T F Szluha
J Turner
Welding Institute
Cambridge, United Kingdom April 1983
- TR 83-26 The KBS UO₂ leaching program
Summary Report 1983-02-01
Ronald Forsyth
Studsvik Energiteknik AB
Nyköping, Sweden February 1983
- TR 83-27 Radiation effects on the chemical environment in a radioactive waste repository
Trygve Eriksen
Royal Institute of Technology
Stockholm, Sweden April 1983

- TR 83-28 An analysis of selected parameters for the BIOPATH-program
U Bergström
A-B Wilkens
Studsvik Energiteknik AB
Nyköping, Sweden April 1983
- TR 83-29 On the environmental impact of a repository for spent nuclear fuel
Otto Brotzen
Stockholm, Sweden April 1983
- TR 83-30 Encapsulation of spent nuclear fuel - Safety Analysis
ES-konsult AB
Stockholm, Sweden April 1983
- TR 83-31 Final disposal of spent nuclear fuel - Standard programme for site investigations
Compiled by
Ulf Thoregren
Swedish Geological
April 1983
- TR 83-32 Feasibility study of detection of defects in thick welded copper
Tekniska Röntgencentralen AB
Stockholm, Sweden April 1983
- TR 83-33 The interaction of bentonite and glass with aqueous media
M Mosslehi
A Lambrosa
J A Marinsky
State University of New York
Buffalo, NY, USA April 1983
- TR 83-34 Radionuclide diffusion and mobilities in compacted bentonite
B Torstenfelt
B Allard
K Andersson
H Kipatsi
L Eliasson
U Olofsson
H Persson
Chalmers University of Technology
Göteborg, Sweden April 1983
- TR 83-35 Actinide solution equilibria and solubilities in geologic systems
B Allard
Chalmers University of Technology
Göteborg, Sweden 1983-04-10
- TR 83-36 Iron content and reducing capacity of granites and bentonite
B Torstenfelt
B Allard
W Johansson
T Ittner
Chalmers University of Technology
Göteborg, Sweden April 1983

- TR 83-37 Surface migration in sorption processes
A Rasmuson
I Neretnieks
Royal Institute of Technology
Stockholm, Sweden March 1983
- TR 83-38 Evaluation of some tracer tests in the granitic
rock at Finnsjön
L Moreno
I Neretnieks
Royal Institute of Technology, Stockholm
C-E Klockars
Swedish Geological, Uppsala
April 1983
- TR 83-39 Diffusion in the matrix of granitic rock
Field test in the Stripa mine. Part 2
L Birgersson
I Neretnieks
Royal Institute of Technology
Stockholm, Sweden March 1983
- TR 83-40 Redox conditions in groundwaters from
Svartboberget, Gideå, Fjällveden and Kamlunge
P Wikberg
I Grenthe
K Axelsen
Royal Institute of Technology
Stockholm, Sweden 1983-05-10
- TR 83-41 Analysis of groundwater from deep boreholes in
Svartboberget
Sif Laurent
Swedish Environmental Research Institute
Stockholm, Sweden April 1983
- TR 83-42 Final disposal of high-level waste and spent
nuclear fuel - foreign activities
R Gelin
Studsvik Energiteknik AB
Nyköping, Sweden May 1983
- TR 83-43 Final disposal of spent nuclear fuel - geological,
hydrological and geophysical methods for site
characterization
K Ahlbom
L Carlsson
O Olsson
Swedish Geological
Sweden May 1983
- TR 83-44 Final disposal of spent nuclear fuel - equipment
for site characterization
K Almén, K Hansson, B-E Johansson, G Nilsson
Swedish Geological
O Andersson, IPA-Konsult
P Wikberg, Royal Institute of Technology
H Ahagen, SKBF/KBS
May 1983

- TR 83-45 Model calculations of the groundwater flow at Finnsjön, själlveden, Gideå and Kamlunge
L Carlsson
Swedish Geological, Göteborg
B Grundfelt
Kemakta Konsult AB, Stockholm
May 1983
- TR 83-46 Use of clays as buffers in radioactive repositories
Roland Pusch
University of Luleå
Luleå May 25 1983
- TR 83-47 Stress/strain/time properties of highly compacted bentonite
Roland Pusch
University of Luleå
Luleå May 1983
- TR 83-48 Model calculations of the migration of radio-nuclides from a repository for spent nuclear fuel
A Bengtsson
B Grundfelt
Kemakta Konsult AB, Stockholm
M Magnusson
I Neretnieks
A Rasmuson
Royal Institute of Technology, Stockholm
May 1983
- TR 83-49 Dose and dose commitment calculations from ground-waterborne radioactive elements released from a repository for spent nuclear fuel
U Bergström
Studsvik Energiteknik AB
Nyköping, Sweden May 1983
- TR 83-50 Calculation of fluxes through a repository caused by a local well
R Thunvik
Royal Institute of Technology
Stockholm, Sweden May 1983
- TR 83-51 GWHRT - A finite element solution to the coupled ground water flow and heat transport problem in three dimensions
B Grundfelt
Kemakta Konsult AB
Stockholm, Sweden May 1983
- TR 83-52 Evaluation of the geological, geophysical and hydrogeological conditions at Fjällveden
K Ahlbom
L Carlsson
L-E Carlsten
O Durano
N-Å Larsson
O Olsson
Swedish Geological
May 1983